



# Census of R Coronae Borealis Stars. I. Infrared Light Curves from Palomar Gattini IR

Viraj R. Karambelkar<sup>1</sup>, Mansi M. Kasliwal<sup>1</sup>, Patrick Tisserand<sup>2</sup>, Kishalay De<sup>1</sup>, Shreya Anand<sup>1</sup>, Michael C. B. Ashley<sup>3</sup>, Alex Delacroix<sup>4</sup>, Matthew Hankins<sup>5</sup>, Jacob E. Jencson<sup>6</sup>, Ryan M. Lau<sup>7</sup>, Dan McKenna<sup>4</sup>, Anna Moore<sup>8</sup>, Eran O. Ofek<sup>9</sup>, Roger M. Smith<sup>4</sup>, Roberto Soria<sup>10,11</sup>, Jamie Soon<sup>8</sup>, Samaporn Tinyanont<sup>12</sup>, Tony Travoignon<sup>8</sup>, and Yuhan Yao<sup>1</sup>

<sup>1</sup> Cahill Center for Astrophysics, California Institute of Technology, Pasadena, CA 91125, USA; [viraj@astro.caltech.edu](mailto:viraj@astro.caltech.edu)

<sup>2</sup> Sorbonne Universites, UPMC Univ. Paris 6 et CNRS, UMR 7095, Institut d'Astrophysique de Paris, IAP, F-75014 Paris, France

<sup>3</sup> School of Physics, University of New South Wales, Sydney, NSW 2052, Australia

<sup>4</sup> Caltech Optical Observatories, California Institute of Technology, Pasadena, CA 91125, USA

<sup>5</sup> Arkansas Tech University, 203 W. O St., Russellville, AR 72801, USA

<sup>6</sup> University of Arizona, Steward Observatory, 933 N. Cherry Ave., Tucson, AZ 85721, USA

<sup>7</sup> Institute of Space and Astronautical Science, Japan Aerospace Exploration Agency, 3-1-1 Yoshinodai, Chuo-ku, Sagami-hara, Kanagawa 252-5210, Japan

<sup>8</sup> Research School of Astronomy and Astrophysics, Australian National University, Canberra, ACT 2611, Australia

<sup>9</sup> Department of Particle Physics and Astrophysics, Weizmann Institute of Science, Rehovot 76100, Israel

<sup>10</sup> College of Astronomy and Space Sciences, University of the Chinese Academy of Sciences, Beijing 100049, People's Republic of China

<sup>11</sup> Sydney Institute for Astronomy, School of Physics A28, The University of Sydney, Sydney, NSW 2006, Australia

<sup>12</sup> University of California Santa Cruz, 1156 High St., Santa Cruz, CA 95064, USA

Received 2020 December 19; revised 2021 February 9; accepted 2021 February 10; published 2021 April 5

## Abstract

We are undertaking the first systematic infrared (IR) census of R Coronae Borealis (RCB) stars in the Milky Way, beginning with IR light curves from the Palomar Gattini IR (PGIR) survey. The PGIR is a 30 cm  $J$ -band telescope with a 25 deg<sup>2</sup> camera that is surveying 18,000 deg<sup>2</sup> of the northern sky ( $\delta > -28^\circ$ ) at a cadence of 2 days. We present PGIR light curves for 922 RCB candidates selected from a mid-IR color-based catalog. Of these 922, 149 are promising RCB candidates, as they show pulsations or declines similar to RCB stars. The majority of the candidates that are not RCB stars are either long-period variables (LPVs) or RV Tauri stars. We identify IR color-based criteria to better distinguish between RCB stars and LPVs. As part of a pilot spectroscopic run, we obtain NIR spectra for 26 of the 149 promising candidates and spectroscopically confirm 11 new RCB stars. We detect strong He I  $\lambda 10830$  features in the spectra of all RCB stars, likely originating within high-velocity (200–400 km s<sup>-1</sup>) winds in their atmospheres. Nine of these RCB stars show <sup>12</sup>C<sup>16</sup>O and <sup>12</sup>C<sup>18</sup>O molecular absorption features, suggesting that they are formed through a white dwarf merger. We detect quasiperiodic pulsations in the light curves of five RCB stars. The periods range between 30 and 125 days and likely originate from the strange-mode instability in these stars. Our pilot run results motivate a dedicated IR spectroscopic campaign to classify all RCB candidates.

*Unified Astronomy Thesaurus concepts:* R Coronae Borealis variable stars (1327); Hydrogen deficient stars (769); Near infrared astronomy (1093); Time domain astronomy (2109)

*Supporting material:* machine-readable table

## 1. Introduction

The R Coronae Borealis (RCB) stars form a distinct class of variable stars (Clayton 2012). These stars are notable for their extreme photometric variations and characteristic chemical compositions. They are characterized by deep, rapid declines in their brightness ( $\approx 9$  mag in the  $V$  band; Clayton 1996) that can last for hundreds of days before they emerge from the low state back to the initial brightness. The RCB stars also belong to the class of hydrogen-deficient stars, with helium being the most abundant element in their atmospheres, followed by carbon, nitrogen, and oxygen (Asplund et al. 2000). Most RCB stars are thought to be remnants of white dwarf (WD) mergers (Webbink 1984; Clayton 2012); however, some could originate from a final helium shell flash in an evolved low-mass star (Iben et al. 1996). Thus, RCB stars are potential low-mass counterparts of Type Ia supernovae in the double-degenerate (DD) scenario (Fryer & Diehl 2008).

The photometric and spectroscopic properties of RCB stars have been studied extensively. While at maximum light, they are known to pulsate with periods between 40 and 100 days and amplitudes of a few tenths of a magnitude (Lawson & Kilkenny 1996). The stars can then undergo mass-loss episodes

that eject “puffs” of dust around them (Feast et al. 1997). If the dust is ejected along the line of sight to a star, its brightness decreases rapidly. The dust is eventually blown away by radiation pressure, and the star rises back to its initial brightness (Clayton et al. 1992). Spectra of RCB stars taken at maximum light suggest that most of them are F- to G-type supergiants (Iben et al. 1996; although a few “hot” RCB stars with  $T > 10,000$  K exist; De Marco et al. 2002; Tisserand et al. 2020). The RCB stars with effective temperatures  $T_{\text{eff}} < 6800$  K show spectra with absorption features of molecules such as CO, CN, and C<sub>2</sub> (Morgan et al. 2003; Tisserand et al. 2020). Most RCB stars do not show any hydrogen features in their spectra. However, a few exceptions exist. The stars V854 Cen, VCra, U Aqr, and DY Cen are relatively more hydrogen-rich, and their spectra show H Balmer lines (Kilkenny & Marang 1989; Lawson & Cottrell 1989). During a photometric decline, the dust-enveloped RCB star shows a mostly featureless spectrum with a few emission lines.

There are two contending theories to explain the formation of RCB stars: DD and final flash (FF). In the DD scenario, RCB stars are proposed to be remnants of the merger of an He-core WD and a CO-core WD. In the FF scenario, they are

proposed to be the product of a final helium flash in the central star of a planetary nebula. The DD scenario is supported by the discovery of large abundances of  $^{18}\text{O}$  in the atmospheres of some RCB stars (Clayton et al. 2007; García-Hernández et al. 2009). Using the CO band head in the near-infrared (NIR) spectra, these studies measured an  $^{16}\text{O}/^{18}\text{O}$  ratio of order unity in several RCB stars. For comparison, this ratio is  $\approx 500$  in the solar system (Geiss et al. 2002). Such high quantities of  $^{18}\text{O}$  can be produced during a WD merger (Clayton et al. 2007; Jeffery et al. 2011). In contrast, there is no such model in the FF scenario that can explain the  $^{18}\text{O}$  overabundance (García-Hernández et al. 2009). However, the FF scenario is supported by the detection of Li and  $^{13}\text{C}$  in a few RCB stars (Asplund et al. 2000; Rao & Lambert 2008). Thus, the DD scenario could account for most of the RCB stars, while a small fraction, those without an  $^{18}\text{O}$  overabundance, may be formed through the FF channel.

There is a big discrepancy between the number of known and predicted Galactic RCB stars. Currently, 117 Galactic RCB stars are known (Tisserand et al. 2020), while the total number is expected to be much larger. Assuming a DD origin with a WD merger rate of  $\approx 10^{-2} \text{ yr}^{-1}$  from Han (1998), Clayton (2012) estimated that there are  $\approx 5400$  RCB stars in the Milky Way. This number is consistent with that extrapolated from the RCB population of the Large Magellanic Cloud (Alcock et al. 2001). From a campaign to identify Galactic RCB stars using mid-IR colors, Tisserand et al. (2020) estimated the total number to be  $\approx 380\text{--}550$ . This suggests a lower WD merger rate of  $\sim 10^{-3} \text{ yr}^{-1}$ , which is consistent with theoretical estimates made from population synthesis via the DD channel (Ruiter et al. 2009; Karakas et al. 2015). An accurate estimate of the number of RCB stars is important to shed further light on their progenitors. In the DD scenario, this number will provide an independent probe of the rate of mergers of WD binaries. This will be particularly useful, as close WD binaries will be important gravitational-wave sources for LISA (Amaro-Seoane et al. 2017; Burdge et al. 2020).

Modern time domain surveys provide an attractive avenue for resolving this discrepancy. The high-cadence, long-baseline photometric observations are ideal to flag RCB stars (from their declines). These can be further followed up spectroscopically to study their chemical compositions. Such studies have been carried out in the past with data from optical surveys such as the Massive Compact Halo Object project (MACHO; Alcock et al. 2001; Zaniwsky et al. 2005), EROS-2 (Tisserand et al. 2004, 2008, 2009), the Catalina Survey (Lee 2015), the All Sky Automated Survey for Supernovae (ASAS-SN; Tisserand et al. 2013; Otero et al. 2014; Shields et al. 2019), and the Zwicky Transient Facility (ZTF; Lee et al. 2020). In this paper, we use data from the Palomar Gattini IR (PGIR), an IR time domain facility to conduct the first NIR search for RCB stars.

The PGIR (De et al. 2020b; Moore & Kasliwal 2019) is a  $25 \text{ deg}^2$   $J$ -band camera on a 30 cm telescope located atop Mt. Palomar. The PGIR was commissioned in 2018 September and commenced survey operations in 2019 July. It surveys the entire northern sky ( $18,000 \text{ deg}^2$ ;  $\delta > -28^\circ$ ) to a depth of  $J \approx 16$  mag (AB) and a cadence of  $\approx 2$  days. In the Galactic plane, the limiting magnitude drops to  $J \approx 14$  mag (AB) due to confusion noise. The RCB stars are inherently brighter in the  $J$  band compared to the optical. Of all known Galactic RCB stars, 95% have Two Micron All Sky Survey (2MASS)  $J$ -band magnitudes brighter than 14 mag. Even during a photometric

decline, the  $J$ -band brightness decreases by  $\approx 3$  mag (Feast et al. 1997), as opposed to 9 mag in the optical. Of the known Galactic RCB stars, 66% are brighter than 11 mag in the  $J$  band. This puts a majority of the Galactic RCB stars above the sensitivity of the PGIR. Additionally, a large number of RCB stars are expected to be located toward the Galactic center, in regions of high dust extinction (Tisserand et al. 2020). The extinction due to dust is significantly lower in the IR compared to optical wavelengths. This makes the PGIR an ideal instrument to conduct a systematic search for Galactic RCB stars. In the first part of this search, we focus on PGIR  $J$ -band light curves for objects in a preexisting catalog of candidate Galactic RCB stars (Tisserand et al. 2020).

The remainder of this paper is structured as follows. In Section 2, we describe our source catalog and present PGIR  $J$ -band light curves of 922 objects from this catalog. We use the light curves to identify promising RCB candidates from contaminants such as long-period variables (LPVs) and RV Tauri stars. In Section 3, we use our light curve-based classifications to identify IR color criteria to distinguish between RCB stars and LPVs to subsequently prioritize our spectroscopic follow-up. In Section 4, we present results from a pilot NIR spectroscopic campaign to identify new RCB stars from our list. In Section 5, we analyze the NIR spectra and light curves of several RCB stars to derive their radial velocities, photospheric temperatures,  $^{16}\text{O}/^{18}\text{O}$  ratios, and pulsation periods and discuss the implications of these quantities on their formation channels. We conclude with a summary of our results and future prospects in Section 6.

## 2. IR Light Curve-based Prioritization

Our source catalog comes from the Tisserand et al. (2020) list of 2194 Galactic RCB candidates selected based on their Wide-field Infrared Survey Explorer (WISE) colors. We performed forced aperture photometry using a 3 pixel ( $\approx 13''$ ) aperture on all  $J$ -band PGIR images since 2018 November at the locations of these candidates to generate light curves for each of them. The average cadence between observations is  $\approx 2$  days. The baseline of observations is  $\approx 500$  days, which corresponds to two observing seasons of the Galactic plane. Further details of the imaging and photometric pipeline can be found in De et al. (2020b). We note that the photometric data taken before (after) May 2020 for sources brighter than  $J \approx 8.5$  (6) mag may not be accurate due to nonlinearity effects in the detector (De et al. 2020a).

Of the 2194 targets of interest, 1209 sources lie in the on-sky area covered by PGIR ( $\delta \gtrsim -28^\circ$ ). Of these, 287 are fainter than the detection limit of PGIR. The remaining 922 sources have  $J$ -band light curves. In addition to RCB stars, this list also contains several contaminants. These mainly include Miras, dust-enshrouded RV Tauri stars, and T Tauri stars (see Section 2.4 in Tisserand et al. 2020). Miras are LPVs with periods longer than 150 days. The RV Tauri and T Tauri stars show pulsations on timescales of a few weeks (Grankin et al. 2007). In this aspect, their light curves are similar to RCB stars at maximum light. However, unlike RCB stars, some RV Tauri stars show subsequent deep and shallow minima. Some also exhibit a long-term periodic trend in addition to the shorter periodic variations.<sup>13</sup> To weed out these periodic impostors, we fit sinusoids to the  $J$ -band light curves of all candidates using

<sup>13</sup> [http://ogle.astrouw.edu.pl/atlas/RV\\_Tau.html](http://ogle.astrouw.edu.pl/atlas/RV_Tau.html)

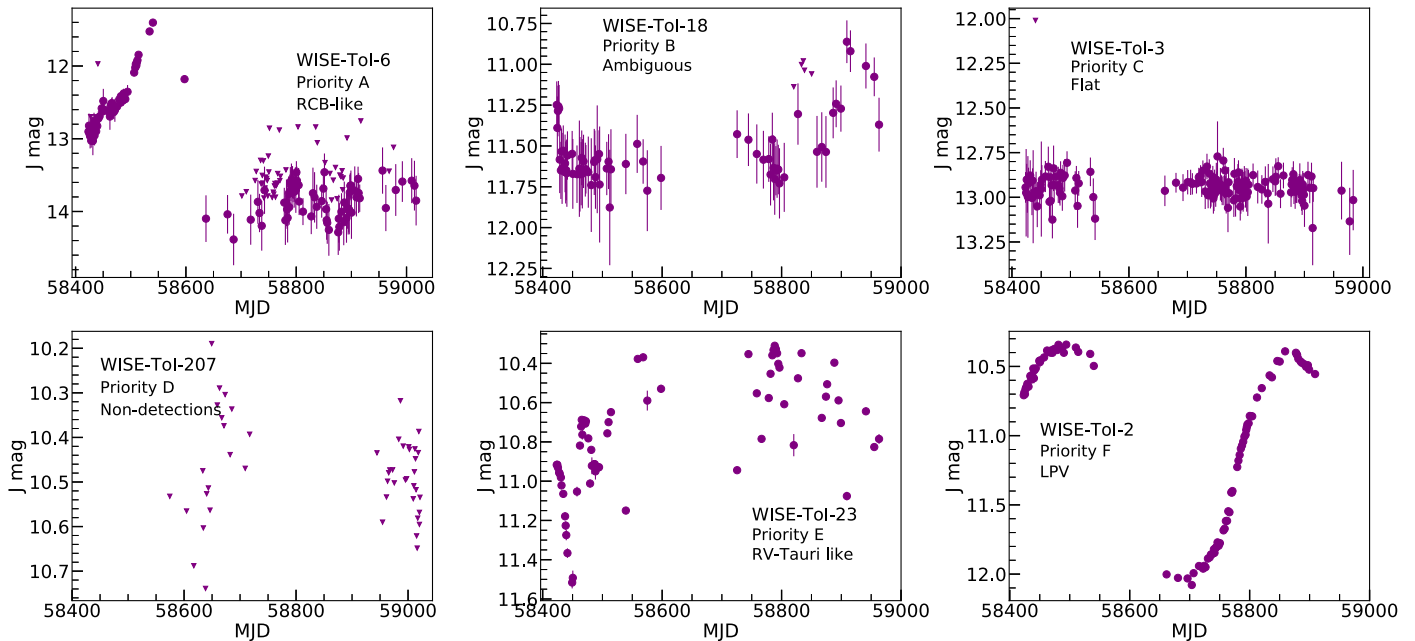


**Figure 1.** Examples of PGIR  $J$ -band light curves for candidates in each of the light curve-based priority groups described in Section 2. The filled dots represent detections, and the triangles represent  $5\sigma$  upper limits. Of the 1209 candidates from the Tisserand et al. (2020) catalog that have PGIR coverage, we assign 149 candidates priority A (RCB-like), 279 candidates priority B (ambiguous light curves), 199 candidates priority C (flat light curves), 287 candidates priority D (no detections), 23 candidates priority E (RV Tauri-like) and 272 candidates priority F (LPV-like). The priority A group is expected to be rich in RCB stars, but groups B, C, and D could also contain RCB stars.

the GATSPY (VanderPlas & Ivezić 2015) implementation of the Lomb–Scargle (LS) method (Lomb 1976; Scargle 1982). We visually examine the fits to determine the reliability of the derived period.

With this information in hand, we find that the 1209 candidates can be divided into the following priority groups based on their PGIR light curves.

1. *Priority A.* The light curve shows sharp, deep declines or rises or pulsations at timescales of a few weeks and resembles that of an RCB star. We identify 149 candidates in this category. We further divide this category into three subcategories based on the trends shown by their light curves as of 2020 July: 48 candidates that are declining, 53 candidates that are rising, and 48 candidates that are pulsating (with periods  $\lesssim 100$  days).
2. *Priority B.* The light curve is ambiguous, not sufficient for any firm classification. There are 279 candidates in this category. Of these, 58 show an overall rise in their brightness, and 44 show an overall decline. Twenty-nine candidates have too-large photometric errors to identify any trend, and 148 sources show erratic photometric variations.
3. *Priority C.* The light curve shows no significant photometric evolution ( $< \approx 0.1$  mag) for the last 500 days. There are 199 candidates in this category.
4. *Priority D.* There are no detections in the PGIR data; 287 candidates belong in this category.
5. *Priority E.* The light curve is consistent with that of an RV Tauri or a T Tauri star. Twenty-three candidates belong in this category.
6. *Priority F.* The light curve is consistent with an LPV. There are 272 candidates in this category.

The groups are listed in order of priority for spectroscopic follow-up. Figure 1 shows examples of light curves in each priority group. The priority A group is expected to be rich in

**Table 1**  
Light Curve-based Priorities, Subclassifications, and IR Color-based Priorities for Spectroscopic Follow-up of Candidates in the Tisserand et al. (2020) Catalog

WISE ToI	R.A. (deg)	Decl. (deg)	Light Curve-based Priority	Light Curve-based Subclass	IR Color-based Priority
1	2.1755	63.0093	A	Pulsating	1-b
2	4.7942	52.0343	F		1-a
3	7.3382	64.8141	C		1-a
4	9.7554	59.4681	B	Erratic	1-a
5	11.6178	58.9057	C		1-a
6	12.0930	74.2992	A	Declining	1-b
...					

**Note.** We assign color-based priorities to all 2194 candidates in the catalog and light curve-based priorities to 1209 candidates that have PGIR coverage.

(This table is available in its entirety in machine-readable form.)

RCB stars. Some objects in this group could be LPVs that show nonsinusoidal variations. The priority B, C, and D groups are also expected to contain RCB stars. Additional PGIR observations will help identify candidates with RCB-like declines or pulsations in these groups. Table 1 lists the light curve-based priorities and subpriorities for each of the 1209 candidates. All 1209 light curves are publicly available online at Zenodo:[10.5281/zenodo.4480376](https://zenodo.org/record/4480376).

### 3. IR Color-based Prioritization

In Section 2, we prioritized 1209 of the 2194 candidates from Tisserand et al.’s (2020) catalog based on their PGIR light curves. Importantly, we identified 272 LPVs and 23 RV Tauri

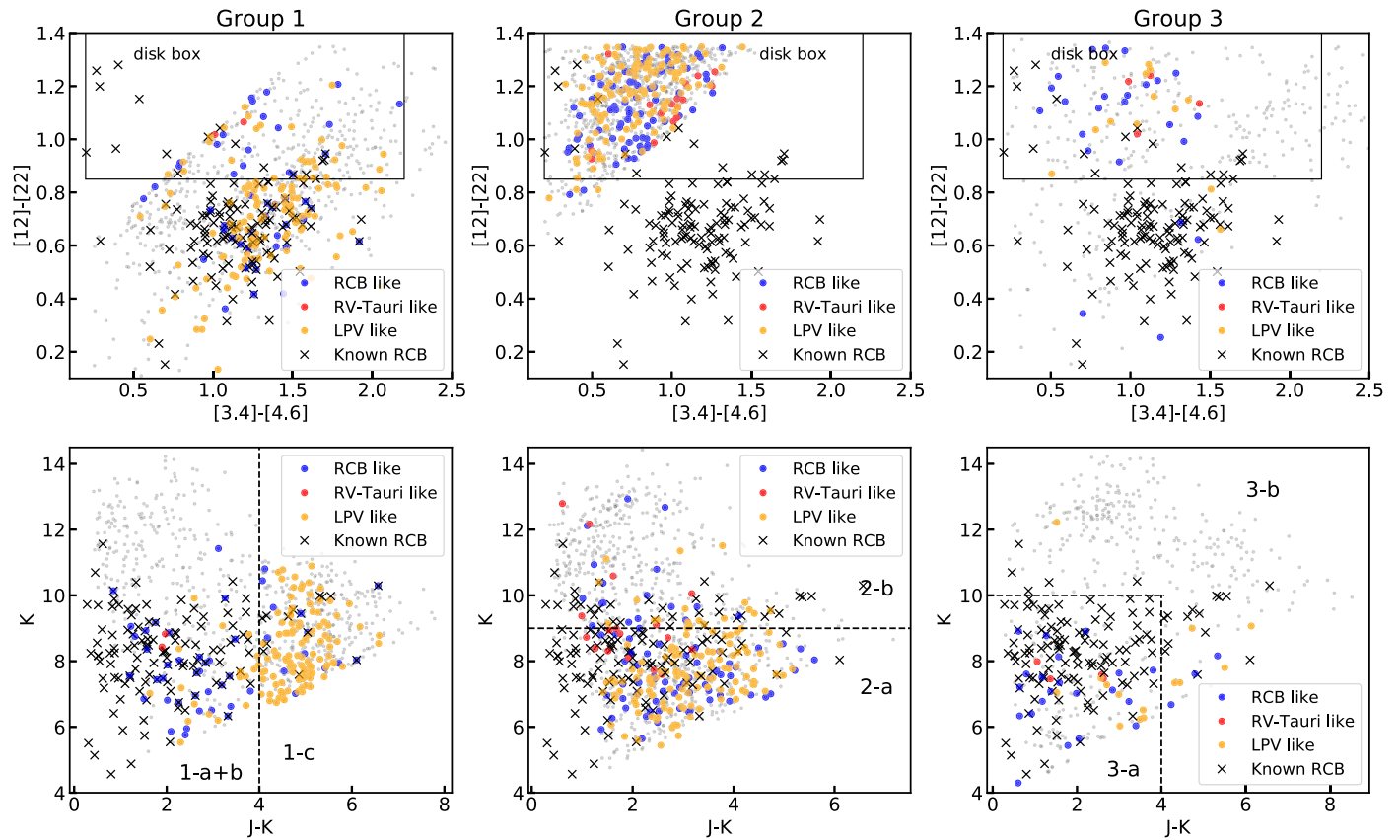


**Figure 2.** The WISE [3.4]–[4.6] vs. [12]–[22] and 2MASS  $K$  vs.  $J - K$  color–color diagrams for all candidates in the Tisserand et al. (2020) catalog. The left column shows the plots for candidates in group 1, the middle column shows candidates in group 2, and the right column shows candidates in group 3. All candidates in each group are plotted as gray background points. In each color–color diagram, we highlight candidates that have light curves similar to RCB stars (priority A; blue circles), RV Tauri stars (priority E; red circles), and LPVs (priority F; orange circles) present in the respective group. In addition, we also plot all known RCB stars as black crosses. We assign a new color-based priority to each candidate based on its position in the  $K$  vs.  $J - K$  diagram, as indicated. In the WISE color–color plots, we also indicate the disk box, where RV Tauri stars surrounded by dust disks are expected to lie (Gezer et al. 2015). In group 1, the  $J - K = 4$  line separates the LPVs from the known RCB stars and light-curve priority A candidates. We assign all candidates in group 1 that have  $J - K < 4$  mag and lie outside the RV Tauri disk box to group 1-a and those inside the disk box to group 1-b. For groups 2 and 3, we cannot identify a similar distinction between LPVs and RCB candidates. Instead, we use the positions of known RCB stars and our light curve-based priority A candidates to prioritize these groups for spectroscopic follow-up (see text). We prioritize candidates in groups 1-a, 2-a, and 3-a for spectroscopic follow-up.

stars from their light curves. Here we explore the positions of these contaminants in the WISE and 2MASS color diagrams. We use this to identify color criteria that distinguish between RCB stars, LPVs, and RV Tauri stars. We then assign a color-based priority to each of the 2194 candidates to optimize further NIR spectroscopic follow-up. This priority will be particularly useful for the 985 candidates that do not have PGIR coverage.

The WISE and 2MASS color–color diagrams were used previously by Tisserand et al. (2020) to divide their catalog into different groups (their Figure 4). Group 1 occupies the bottom right region in the WISE [3.4]–[4.6] versus [12]–[22] diagram. This group is expected to contain the maximum number of RCB stars. Group 2 occupies the top left region in the diagram and is expected to contain rare RCB stars that are surrounded by thin or cold dust shells ( $T < 500$  K). Finally, group 3 comprises objects that are reported with upper limits in at least one WISE band and objects that have prior classifications. We analyze the candidates in each of these groups separately.<sup>14</sup>

Figure 2 shows the WISE [3.4]–[4.6] versus [12]–[22] and 2MASS  $K$  versus  $J - K$  color–color diagrams for all 2194

candidates in the source catalog. We plot these diagrams separately for groups 1, 2, and 3. All candidates in a group are plotted as gray background points. In each panel, we highlight the candidates with light curve-based priority A (RCB-like; blue circles), priority E (RV Tauri; red circles), and priority F (LPVs; orange circles). We also indicate the positions of known RCB stars in these diagrams (black crosses). In the [3.4]–[4.6] versus [12]–[22] diagram, we also mark the “disk box” region, which is expected to contain RV Tauri stars with dust disks around them (Gezer et al. 2015). We note that our light-curve priority E (RV Tauri) candidates lie in this region.

Based on these diagrams, we assign a color-based classification to each of the 2194 candidates as follows.

1. *Group 1.* This group has 785 candidates and is expected to contain the maximum number of RCB stars. The left column in Figure 2 shows the color–color diagrams for candidates in this group. These candidates lie in the bottom right part of the [3.4]–[4.6] versus [12]–[22] diagram. We first note that the  $K$  versus  $J - K$  diagram can be used to separate most LPVs from RCB stars in this group. If we apply a cut of  $J - K < 4$  mag, we eliminate 90% of the LPVs while retaining 90% of the known RCB stars and 73% of the priority A candidates. We assign all

<sup>14</sup> Tisserand et al. (2020) further divided groups 1 and 3 into two subgroups each.

422 candidates with  $J - K > 4$  mag the priority group 1-c. For the few RCBs stars lying within this group, the 2MASS observations were likely obtained while they were in a deep decline phase and consequently being highly reddened. Of the remaining 363 candidates, 111 candidates lie in the RV Tauri disk box. We assign priority group 1-b to these stars. We give the highest priority for spectroscopic follow-up to the remaining 252 candidates: group 1-a.

2. *Group 2.* This group has 987 candidates and is expected to have the highest contamination. The middle column in Figure 2 shows the color–color diagrams for candidates in group 2. These candidates lie in the top left part of the [3.4]–[4.6] versus [12]–[22] diagram. Although this group contains the largest number of candidates, very few known RCB stars (seven out of 117) lie in this region of the diagram. The disk box is not a particularly useful metric for prioritization, as almost all of these candidates lie in the disk box. Unlike group 1, no clear distinction can be made between the LPVs, known RCB stars, and photometric RCB candidates in the  $K$  versus  $J - K$  diagram. If we apply a cut of  $K < 9$  mag, we retain 70% of the known RCB stars and 75% of the light-curve priority A candidates. In the absence of any other criteria, we prioritize the sources with  $K < 9$  mag over the remaining candidates. We assign 548 candidates with  $K < 9$  mag to the higher-priority group 2-a and the remaining 439 candidates to the lower-priority group 2-b.
3. *Group 3.* This group has 422 candidates. The right column in Figure 2 shows the color–color diagrams for candidates in group 3. Based on the  $K$  versus  $J - K$  diagram, we prioritize sources that lie inside the box defined by  $4 < K < 10$  and  $J - K < 4$  mag. This box contains 85% of the known RCB stars, 88% of the priority A candidates, and only 50% of the LPVs. We assign 150 candidates that lie in this box priority group 3-a and the remaining 272 candidates group 3-b.

We list these candidates with their color-based priorities in Table 1. For spectroscopic follow-up, we prioritize candidates in groups 1-a, 2-a, and 3-a in decreasing order. Group 1-b is also expected to contain RCB stars but is likely contaminated by RV Tauri stars. The IR colors thus provide an additional metric to prioritize the candidates for spectroscopic follow-up.

Our spectroscopic campaign focuses on candidates in the northern hemisphere that lie in the area covered by the PGIR. First, we aim to spectroscopically follow up all 149 candidates that have light curve-based priority A. From the 765 candidates that have light-curve priority B, C, or D, we will follow up only 241 candidates that belong to our top three IR color-based groups (groups 1-a, 2-a, and 3-a). This leaves us with a sample of 390 candidates for spectroscopic follow-up. The distribution of the candidates among the different priority groups is illustrated in Figure 3.

#### 4. Pilot NIR Spectroscopic Follow-up

In Sections 2 and 3, we reprioritized candidates in the Tisserand et al. (2020) catalog based on their IR light curves and colors. We aim to spectroscopically follow up the candidates in the top priorities to confirm their true nature. Traditionally, large-scale spectroscopic campaigns for identifying RCB stars have made use of optical spectra. As noted in

Section 1, RCB stars are significantly brighter in the NIR compared to the optical. Thus, NIR wave bands are better suited to efficiently observe a large number of candidate RCB stars. In addition, NIR spectral features such as the  $^{12}\text{C}^{16}\text{O}$  and  $^{12}\text{C}^{18}\text{O}$  band heads can provide useful diagnostics about the progenitors of these stars. Thus, an NIR spectroscopic campaign promises to be highly productive in identifying and characterizing RCB stars. No such campaign has been conducted in the past. As a pilot for such a campaign, we obtained NIR spectra for eight known RCB stars and 31 of our top light curve-based priority candidates. Of the 31 candidates, 26 have light-curve priority A, and five have light-curve priority B. Here we present the results from this pilot run.

We used Triplespec (Herter et al. 2008), a medium-resolution ( $R \approx 2700$ ) *JHK*-band spectrograph on the 200 inch Hale telescope at Mt. Palomar. We observed eight known RCB stars and 21 candidates on 2019 October 23 and three additional candidates on 2020 February 3. We further observed seven more candidates on 2020 June 28 with the Spex spectrograph ( $R \approx 1500$ ) on the NASA Infrared Telescope Facility (IRTF; Rayner et al. 2003) at Maunakea. The IRTF observations were acquired as part of program 2020A111 (PI: K. De). All spectra were extracted using the IDL package `spextool` (Cushing et al. 2004). The extracted spectra were flux-calibrated and corrected for telluric absorption with standard star observations using `xtellcor` (Vacca et al. 2003).

##### 4.1. NIR Spectral Features of Known RCB Stars

We obtained NIR spectra of eight known RCB stars (as listed on SIMBAD<sup>15</sup>): AO Her, V391 Sct, NSV 11154, WISE J184158.40–054819.2 (WISE J18+), WISE J175749.76–075314.9 (WISE J17+), ASAS-RCB-21, WISE J194218.38–203247.5 (WISE J19+), and ASAS-RCB-20.

Figure 4 shows the  $J$ -band light curves of these stars. Seven of the known RCB stars have been reported as cold ( $T_{\text{eff}} < 6800$  K): AO Her (P. Tisserand, private communication), NSV 11154 (Kijbunchoo et al. 2011), ASAS-RCB-20, ASAS-RCB-21 (Tisserand et al. 2013), WISE J17+, WISE J18+, and WISE J19+ (Tisserand et al. 2020). The star V391 Sct has been reported as a warm RCB by Tisserand et al. (2013). Four out of the eight RCB stars—V391 Sct, NSV 11154, AO Her, and WISE J18+—were at the maximum-light phase when the spectra were obtained. All four stars exhibit quasiperiodic pulsations with periods between 40 and 140 days. The RCB stars WISE J19+ and ASAS-RCB-20 were in the photometric minimum phase. The stars WISE J17+ and ASAS-RCB-21 were rising out of a photometric minimum toward maximum light. Figure 5 shows the NIR spectra of these stars, grouped by their photometric phase. We note the following characteristic features in these spectra.

1. All RCB stars show He I ( $\lambda 10830$ ) emission or absorption features. The two stars inside a photometric minimum show helium emission. The emission is strong for WISE J19+ (just entering the minimum) and very weak for ASAS-RCB-20 (deep inside the minimum, featureless spectrum). The pulsating and rising stars show either a fully developed P Cygni profile or strong blueshifted absorption. We discuss the He I line profiles in more detail in Section 5.3.

<sup>15</sup> <https://simbad.u-strasbg.fr>

Light curve based priorities for 1209 candidates

	Priority A RCB-like 149	Priority B ambiguous 279	Priority C flat 199	Priority D no detect. 287	Priority E RV-Tauri 23	Priority F LPV 272	
IR color based priorities for 2194 candidates	1-a 252	21	38	37	34	0	11
	1-b 111	14	18	10	11	2	7
	1-c 422	13	33	22	87	0	106
	2-a 548	58	72	1	13	11	114
	2-b 439	19	55	91	48	6	20
	3-a 101	21	39	5	2	4	8
	3-b 321	3	24	33	92	0	6

**Figure 3.** Schematic of light curve-based and IR color-based priorities for RCB candidates. We assign light curve-based priorities (A–F) to 1209 of the 2194 candidates in the Tisserand et al. (2020) catalog. We also divide the full catalog into seven groups based on the IR colors of the candidates. In this figure, we indicate the overlap between each light curve-based and IR color-based group. For our campaign, we aim to observe all 149 candidates with light-curve priority A. We will also observe 241 additional candidates that have light-curve priorities B, C, and D and belong to IR color groups 1-a, 2-a, and 3-a. We highlight these 390 candidates in green.

- The RCB stars inside a minimum show a mostly featureless reddened spectrum with He I emission. If the star has entered the minimum recently, other emission lines, such as Si I and C<sub>2</sub>, are detected. These features are absent if the star is deep inside the minimum.
- The rising and pulsating RCB stars show a variety of atomic absorption lines. These include C I (most prominently at 1.0686 and 1.0688  $\mu\text{m}$ ), along with Fe I, Si I, and K I.
- Of the rising and pulsating RCB stars, all but V391 Sct show the CN (1.0875, 1.0929, 1.0966, and 1.0999  $\mu\text{m}$ ) and <sup>12</sup>C<sup>16</sup>O (2.2935, 2.3227, 2.3525, 2.3829, and 2.4141  $\mu\text{m}$ ) absorption band heads. The presence of these molecular band heads suggests that these stars have cold photospheres ( $T_{\text{eff}} < 6800$  K). Importantly, we also detect <sup>12</sup>C<sup>18</sup>O absorption features in the K band of all of these stars. We discuss the CO band head in more detail in Section 5.1.2.
- None of the eight RCB stars show any hydrogen features in their NIR spectra.

#### 4.2. New RCB Stars

We obtained NIR spectra for 31 RCB candidates, 26 with light-curve priority A and five with light-curve priority B. None of the five priority B candidates show spectra resembling RCB stars. Of the 26 priority A candidates, we identify 11 new RCB stars using the spectral features described in Section 4.1. These stars are WISE ToI 6, 8, 222, 223, 225, 268, 274, 281, 1213,

1225, and 1309. Table 2 summarizes the properties of these stars. Figure 6 shows the light curves of these stars, and Figure 7 shows their spectra. Here we discuss the properties of these newly identified RCB stars. We group the stars by their photometric phase at the time the spectra were obtained.

##### 4.2.1. Declining

Seven of the 11 new RCB stars—WISE ToI 6, 222, 225, 268, 281, 1213, and 1225—were in a photometric minimum or undergoing a photometric decline when the spectra were obtained. The light curves of WISE ToI 6, 222, 225, and 1225 indicate that these stars were in a photometric minimum for more than 100 days before the spectra were taken. These stars showed photometric declines of  $\approx 3$  mag in the *J* band and present featureless spectra with strong He I emission. WISE ToI 268 and 281 show shallower declines ( $\approx 1.5$  mag) and also brief recoveries from the declines. Their spectra show strong blueshifted He I absorption and <sup>12</sup>C<sup>16</sup>O and <sup>12</sup>C<sup>18</sup>O absorption bands, suggesting that they are cold RCB stars. The light curve of WISE ToI 1213 shows a complex photometric evolution where the star underwent shallow declines and recoveries of 1 mag and a deep decline of  $> 3$  mag. The spectrum obtained during this decline shows He I with a P Cygni profile. We also detect the <sup>12</sup>C<sup>16</sup>O absorption band head with traces of <sup>12</sup>C<sup>18</sup>O, suggesting that this is a cold RCB star.

We note that WISE ToI 225, 222, and 281 lie in highly extinguished regions of the Galaxy. The integrated line-of-sight extinction in their direction ( $A_V$ ) is 6.5, 8.7, and 22 mag,

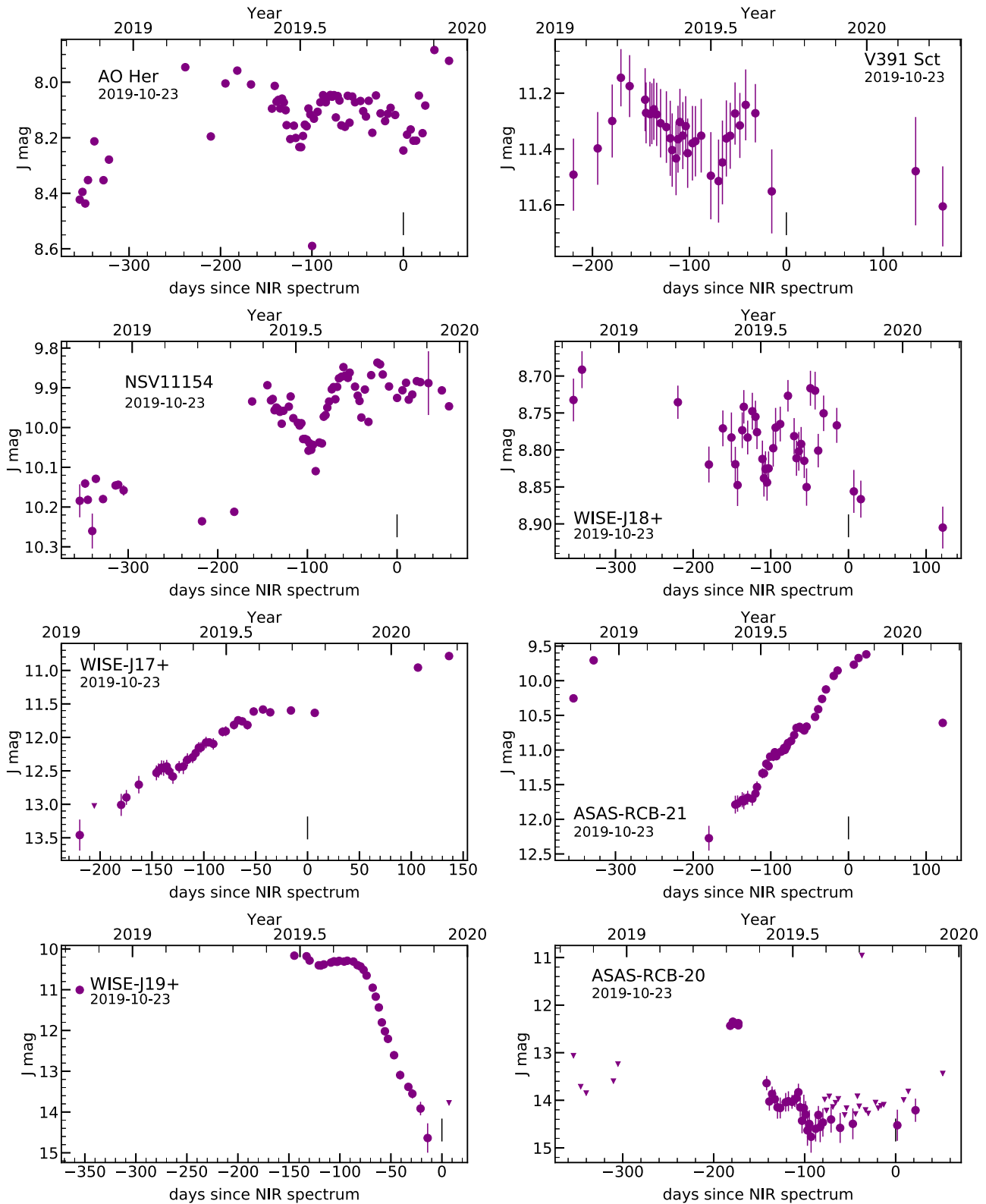


**Figure 4.** The PGIR  $J$ -band light curves for eight known RCB stars. The black vertical lines at zero days mark the epoch at which the NIR spectra were acquired (indicated in each plot). We note that photometry brighter than 8.5 mag may not be reliable due to nonlinearity effects in the detector. The  $J$ -band magnitudes are in the Vega system.

respectively (Schlafly & Finkbeiner 2011). Their 2MASS  $J$ -band magnitudes are 10.8, 9.0, and 10.9 mag, and their PanSTARRS  $g$ -band magnitudes are 19.9, 20.2, and 22.4 mag, respectively.

These stars thus have  $J - g \gtrsim 10$  mag and illustrate the advantage that NIR searches offer over even very deep optical searches for RCB stars.

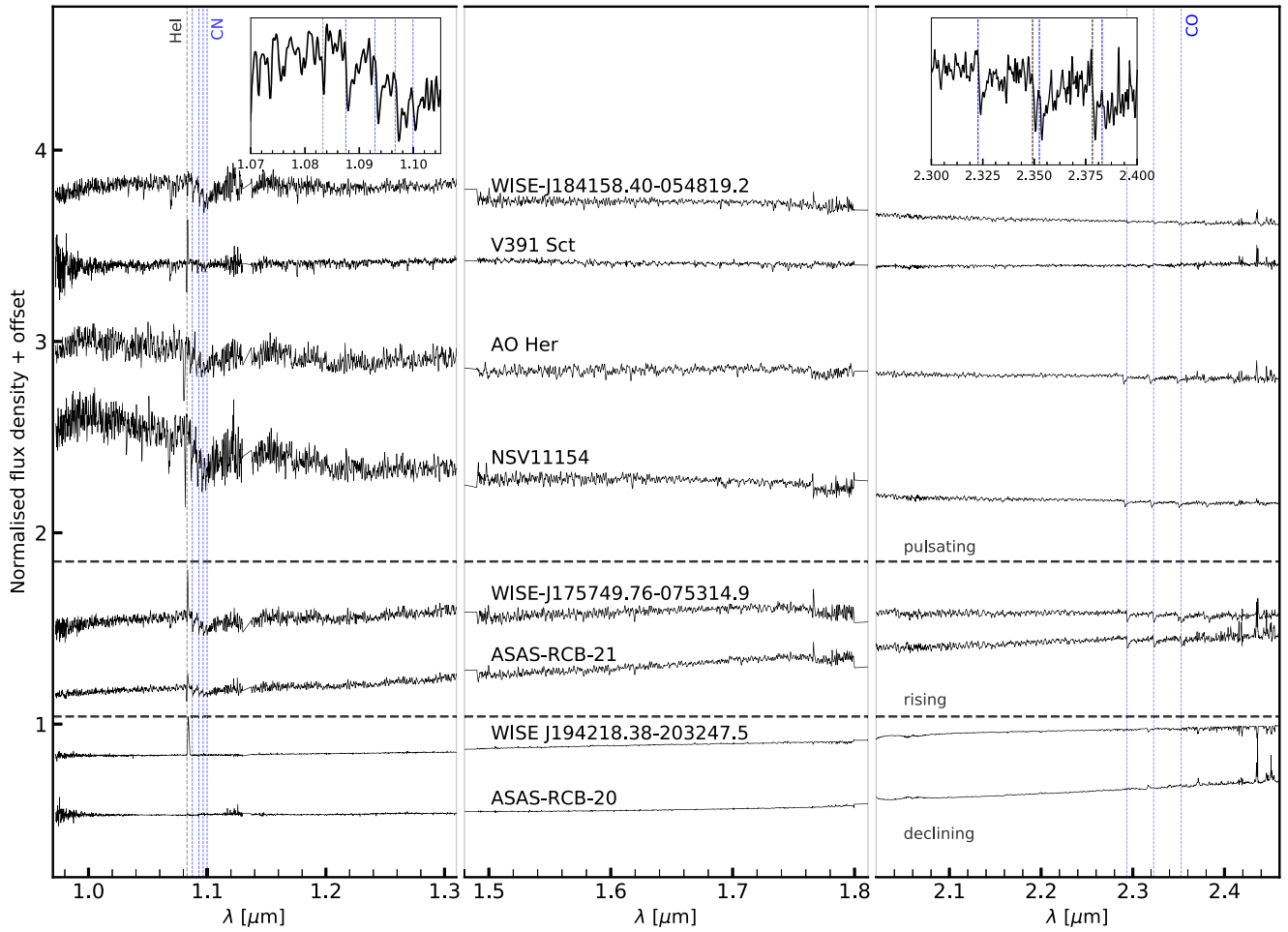


**Figure 5.** The NIR spectra of eight known RCB stars on 2019 November 23. The stars are grouped by their photometric phase: four pulsating, two rising, and two fading. We also show a zoom-in of the  $J$ - and  $K$ -band spectra of the RCB star WISE J18+. In the  $J$ -band inset plot, we mark the positions of the CN absorption band head in blue and the He I absorption in gray. In the  $K$ -band inset, we mark the positions of the  $^{12}\text{C}^{16}\text{O}$  and  $^{12}\text{C}^{18}\text{O}$  absorption band heads in blue and black, respectively.

**Table 2**  
Properties of Newly Identified RCB Stars

WISE Name	WISE ToI	R.A. (deg)	Decl. (deg)	Light-curve Phase <sup>a</sup>	Temperature	$A_V^b$ (mag)	Comments
J004822.34+741757.4	6	12.0931	74.2993	Declining	Cold	4.3	
J005128.08+645651.7	8	12.8670	64.9477	Pulsating	Hot	1.2	Pulsating with period $\approx 30$ days
J181836.38-181732.8	222	274.6516	-18.2925	Declining		8.7	
J182010.96-193453.4	223	275.0457	-19.5815	Rising	Cold	4.9	
J182235.25-033213.2	225	275.6469	-3.5370	Declining		6.5	
J190813.12+042154.1	268	287.0547	4.3650	Declining	Cold	6.8	
J191243.06+055313.1	274	288.1795	5.8870	Rising	Cold	7.7	Sharp rise out of a decline
J192348.98+161433.7	281	290.9541	16.2427	Declining	Cold	22	
J170552.81-163416.5	1213	256.4701	-16.5713	Declining		1.3	
J173737.07-072828.1	1225	264.4045	-7.4745	Declining		2.8	
J185726.40+134909.4	1309	284.3600	13.8193	Rising	Cold	2.4	Rising from 600 day long minimum

#### Notes.

<sup>a</sup> The photometric phase when the spectrum was obtained.

<sup>b</sup> Line-of-sight extinction; values taken from Schlafly & Finkbeiner (2011).

#### 4.2.2. Rising

Three stars—WISE ToI 223, 274, and 1309—were rising out of a photometric decline when the spectra were obtained. The star ToI 223 was at a constant minimum brightness for 200 days before it rose out of the minimum, brightening by 2.5 mag

in the  $J$  band. The star ToI 274 previously underwent a decline of 2 mag but recovered sharply without flattening at the minimum brightness. This variation is similar to the one observed with DY Per-type stars (Tisserand et al. 2009). The  $J$ -band light curve of ToI 1309 suggests that this star was

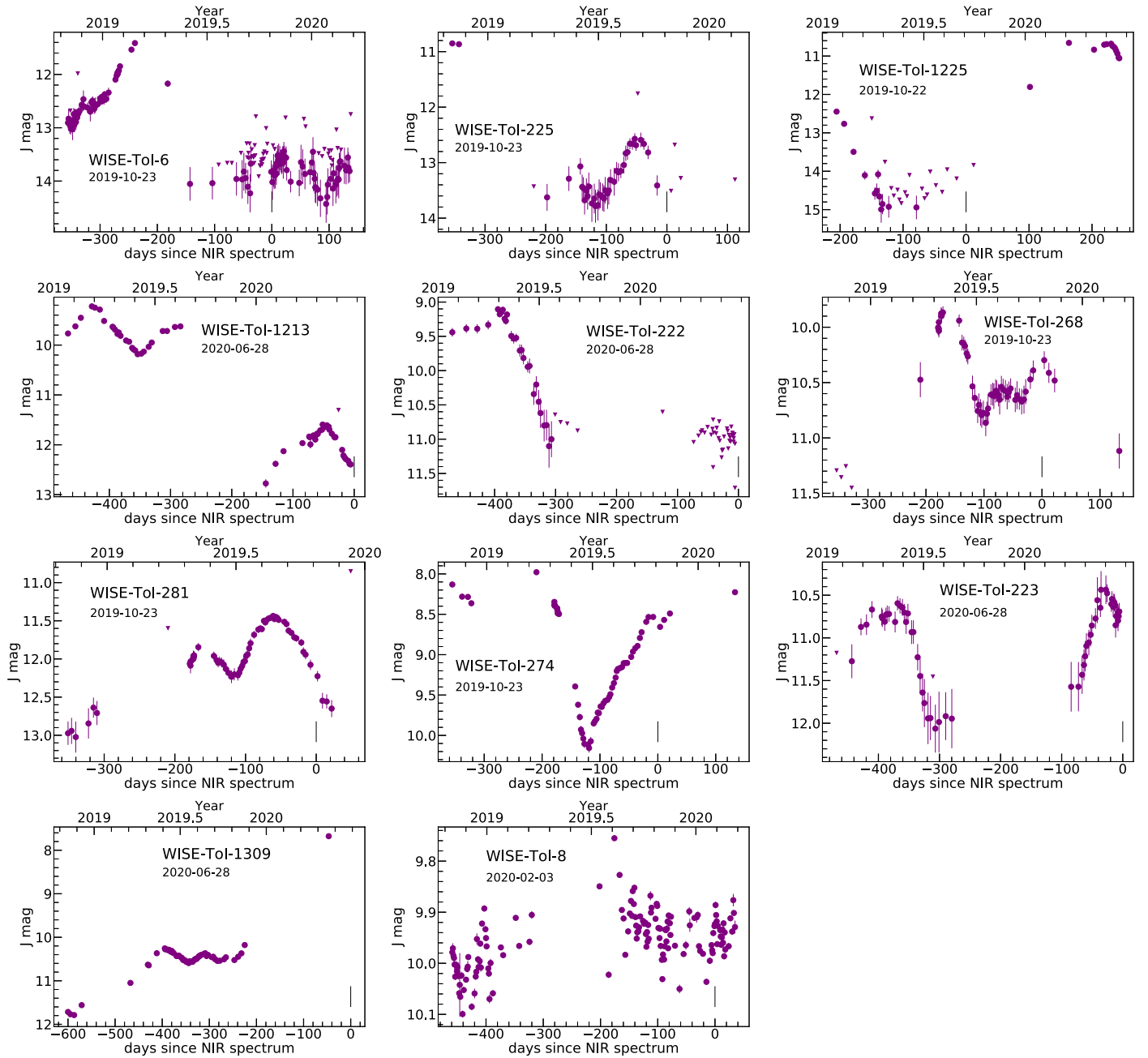


**Figure 6.** The PGIR  $J$ -band light curves of the new RCB stars identified in this paper. The black vertical lines at zero days mark the epochs at which the NIR spectra were acquired. For each RCB star, we also indicate the date when the spectrum was obtained. We note that photometry brighter than 8.5 mag may not be reliable due to nonlinearity effects in the detector. All  $J$ -band magnitudes are in the Vega system.

in a minimum for at least 600 days before our spectrum was obtained. The spectra of these stars show strong blueshifted He I absorption and CN,  $^{12}\text{C}^{16}\text{O}$ , and  $^{12}\text{C}^{18}\text{O}$  absorption features. The star ToI 274 also shows a small redshifted He I emission component.

The stars ToI 223 and 274 have been listed as strong RCB candidates by Tisserand et al. (2020). They noted that these stars are the fifth- and sixth-brightest RCB stars in the  $12\ \mu\text{m}$  band. They have WISE [12] = 1.0 and 1.2 mag, respectively, indicative of a very bright circumstellar dust shell. The integrated Galactic extinction in their direction ( $A_V$ ) is 4.9 and 7.7 mag, respectively, suggesting that they lie in regions of high dust extinction.

#### 4.2.3. Pulsating

The light curve of WISE ToI 8 was showing quasiperiodic variations when the spectrum was obtained. We identify a tentative period of  $\approx 30$  days for this star. This star was photometrically identified as an RCB candidate on AAVSO and by the ASAS-SN survey (Jayasinghe et al. 2018), as it underwent photometric declines in 1999 and 2012. This star has not shown any obvious photometric declines for at least the last 500 days. The spectrum shows blueshifted helium absorption and no hydrogen absorption lines. No CO or CN features are present in our spectrum taken at maximum light, suggesting that this is not a cold RCB star. The spectrum shows several emission lines resembling spectra of hot

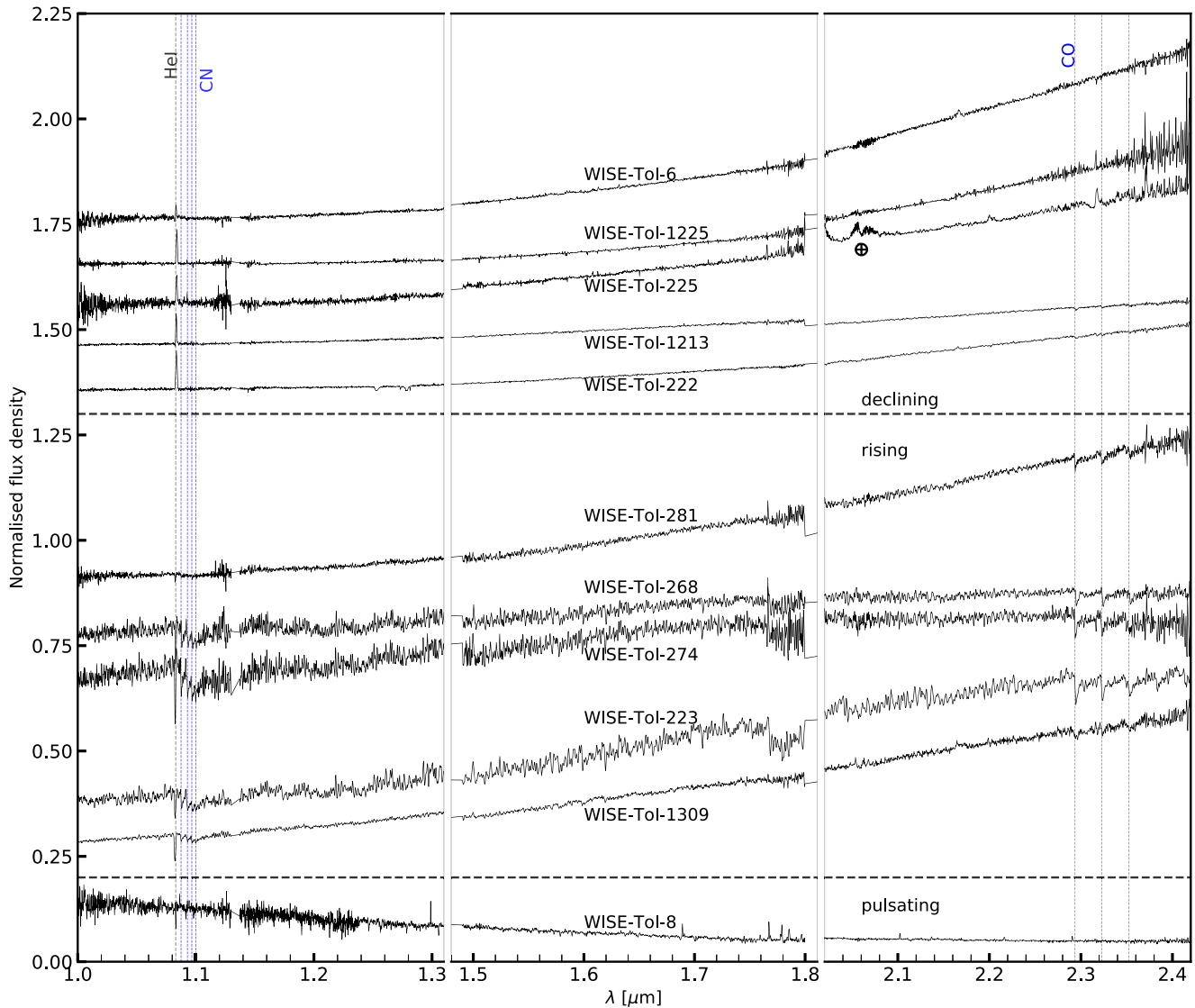


**Figure 7.** The NIR spectra of the new RCB stars identified in this paper. All RCB stars show He I  $\lambda 10830$  features. Five RCB stars that were in a deep decline show strong emission, while others show either fully developed P Cygni profiles or strong blueshifted absorption. Four RCB stars show the CO absorption band head, suggesting that they are cold.

( $T_{\text{eff}} > 10,000$  K) RCB stars. We identify C I emission at  $1.68 \mu\text{m}$ , C II emission at  $1.784 \mu\text{m}$ , Fe II emission at  $1.766$  and  $1.778 \mu\text{m}$ , and, possibly, Ne I emission at  $1.7961 \mu\text{m}$ . Similar to other hot RCB stars, the emission lines are double-peaked, which could indicate the presence of an equatorial outflow around the star (De Marco et al. 2002).

Our pilot campaign has demonstrated the utility of NIR spectra in searches for RCB stars. We will continue this spectroscopic follow-up campaign in the future, aiming for completeness in the top priority classes. The NIR spectra of all RCB stars from our pilot campaign are publicly available online at Zenodo:[10.5281/zenodo.4480376](https://zenodo.org/record/4480376).

## 5. Preliminary Implications for Progenitors

In this paper, we have presented NIR spectra for 19 RCB stars (eight previously known, 11 newly identified). We have also presented long-baseline ( $\approx 500$  days), high-cadence ( $\approx 2$  days) light curves for these stars. In this section, we analyze the NIR spectra to derive diagnostic quantities of the nature of RCB stars. In particular, we focus on photospheric

temperatures, oxygen isotope ratios, and helium line profiles. We also derive maximum-light pulsation periods for five RCB stars. We discuss the implications of these quantities on the progenitors and nature of RCB stars. Although our sample size is not sufficient for any profound insights, the results are indicative of the potential of the NIR campaign. Future observations will increase our sample size and shed more light on the open questions about RCB stars.

### 5.1. Photospheric Temperatures and Isotope Ratios

#### 5.1.1. SED Modeling

We searched archival data from optical, NIR, and mid-IR surveys for maximum-light photometric measurements of the RCB stars analyzed in this paper. For the optical wave bands, we used data from the AAVSO, ZTF, and ASAS-SN sky surveys. For the NIR wave bands, we compare the 2MASS  $J$ -band magnitudes to PGIR light curves to identify RCB stars for which the 2MASS measurements correspond to maximum light. For the mid-IR wave bands, we use the WISE magnitudes

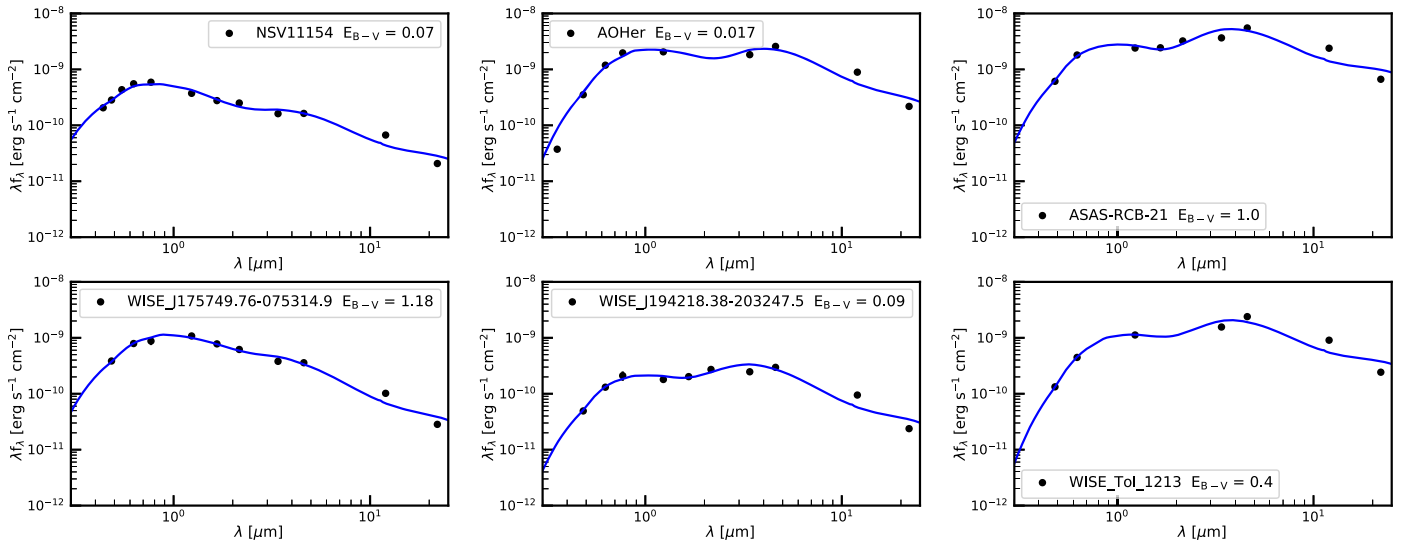


**Figure 8.** Maximum-light SEDs for six RCB stars from our sample. We plot the best-fit DUSTY models in blue. For each star, we also indicate the assumed values of  $E_{B-V}$ . The derived model parameters are listed in Table 3

directly, as the mid-IR fluxes of RCB stars do not vary significantly (Feast et al. 1997). We corrected the WISE 4.6  $\mu\text{m}$  magnitudes for saturation effects based on the prescription in Tisserand (2012). As the distances to these stars are not known accurately ( $\approx 30\%$  uncertainty from Gaia DR2; Bailer-Jones et al. 2018), we cannot estimate the line-of-sight extinction in their direction. We restrict our analysis to only those stars that have integrated  $E_{B-V}$  values smaller than 1.5 mag. We assume 10% uncertainties on the photometric measurements to account for variations in the light curve and uncertainties in extinction. We construct maximum-light spectral energy distributions (SEDs) for six RCB stars analyzed in this paper. This includes five previously known RCB stars—AO Her, NSV 11154, ASAS-RCB-21, WISE J17+, and WISE J19+—and one new RCB, WISE ToI 1213.

We model the SEDs with the radiative transfer code DUSTY (Ivezic & Elitzur 1997; Ivezic et al. 1999; Elitzur & Ivezic 2001). In our models, DUSTY is embedded in a Markov Chain Monte Carlo wrapper using the python package emcee (Foreman-Mackey et al. 2013). We modeled the star as a blackbody corrected for molecular absorption. We used synthetic spectra of RCB stars (see Section 5.1.2) to calculate the molecular absorption fractions. The dust is treated as a shell with a density profile  $\rho \propto r^{-2}$ . We fix the outer radius of the shell to 10 times the inner radius (Clayton et al. 2011). We examine optical depth values in the visual band within the range  $0 < \tau_V < 10$  and dust temperatures in the range  $300 \text{ K} < T_{\text{dust}} < 1200 \text{ K}$ . We assume amorphous carbonaceous dust with a standard MRN size distribution (Mathis et al. 1977). One limitation of this analysis is the assumption of spherical symmetry. Therefore, the estimated dust optical depth could be an over- or underestimation, depending on the viewing angle.

The SEDs and best-fit models from the dust analysis are shown in Figure 8. The model parameters and their  $1\sigma$  uncertainties are listed in Table 3. The stars are consistent with temperatures between 4500 and 6000 K, surrounded by dust shells of temperatures between 700 and 900 K. With improved distance estimates from the next Gaia data release and additional monitoring from optical and NIR surveys, we will be able to estimate the temperatures for several more RCB

stars. Accurate distance measurements will also enable us to derive the luminosities of these stars and place them on the Hertzsprung–Russell diagram.

### 5.1.2. NIR Spectral Modeling

The NIR spectra of cold RCB stars provide a host of information about their compositions. Here we model the CO band head in the  $K$  band to constrain the temperatures and oxygen isotope ratios of these stars. However, the circumstellar dust shells of RCB stars can contribute significantly to the observed  $K$ -band fluxes (up to 80% of the total flux; Tisserand 2012). The observed absorption depth of the CO bands depends largely on the assumed dust contribution. We defer a detailed characterization of the dust shells around these stars to a future paper. Instead, we leave the dust contribution as a free parameter in our model and report a range of effective temperatures and oxygen isotope ratios for these stars. Second, given the medium resolution of our spectra, it is possible that the  $^{12}\text{C}^{16}\text{O}$  band heads of some RCB stars are saturated (García-Hernández et al. 2009). It is thus possible that the values of the oxygen isotope ratios are lower limits for some stars.

We use a grid of hydrogen-deficient spherically symmetric Model Atmospheres in Radiative and Convective Scheme atmospheric models with input compositions characteristic of RCB stars ( $\log \epsilon(\text{H}) = 7.5$ , C/He ratio of 1%; Gustafsson et al. 1975, 2008; Bell et al. 1976; Plez 2008). We generated the synthetic spectra using the package TURBOSPECTRUM (Alvarez & Plez 1998). We set  $\log g = 1.0$  and varied the effective temperatures from 4000 to 7500 K in intervals of 250 K. We chose values of 0.5, 1, 2, 5, 10, 20, 50, 500, and infinity for the  $^{16}\text{O}/^{18}\text{O}$  ratio. We also introduce an additional parameter,  $f_{\text{dust}} = \frac{F_{\text{shell},K}}{F_{\text{total},K}}$ , to quantify the dust shell contribution to the  $K$ -band flux and vary it between zero and 0.8 in steps of 0.1.

We fit the synthetic spectra to the continuum-normalized NIR spectra in the region 2.26–2.4  $\mu\text{m}$ . For each star, we visually selected the spectra that best fit the data for each value of  $f_{\text{dust}}$ . We used these fits to derive upper limits on the photospheric temperature and a range of  $\text{O}^{16}/\text{O}^{18}$  ratios,

**Table 3**  
Properties Derived from the Spectra of RCB Stars

RCB Name	RV <sup>a</sup> (km s <sup>-1</sup> )	$T_{\text{eff}}^b$ (K)	$T_{\text{dust}}^b$ (K)	$\tau_V^b$	$T_{\text{eff}}^c$ (K)	O <sup>16</sup> /O <sup>18c</sup>
AO Her	430 ± 20	4730 <sup>+240</sup> <sub>-200</sub>	830 <sup>+35</sup> <sub>-45</sub>	1.25 <sup>+0.14</sup> <sub>-0.15</sub>	<5750	>10
NSV 11154	260 ± 20	5480 <sup>+140</sup> <sub>-170</sub>	770 <sup>+33</sup> <sub>-35</sub>	0.38 <sup>+0.05</sup> <sub>-0.04</sub>	4750–5750	10–50
WISE J17+	-70 ± 20	4850 <sup>+160</sup> <sub>-130</sub>	830 <sup>+45</sup> <sub>-60</sub>	0.36 <sup>+0.08</sup> <sub>-0.05</sub>	<5750	1–5
ASAS-RCB-21	-100 ± 20	5790 <sup>+300</sup> <sub>-390</sub>	800 <sup>+25</sup> <sub>-35</sub>	2.10 <sup>+0.16</sup> <sub>-0.22</sub>	<6250	2–50
WISE J19+	-50 ± 50	5440 <sup>+350</sup> <sub>-350</sub>	920 <sup>+30</sup> <sub>-50</sub>	1.67 <sup>+0.16</sup> <sub>-0.21</sub>		
WISE ToI 1213	-50 ± 50	4980 <sup>+360</sup> <sub>-400</sub>	790 <sup>+40</sup> <sub>-60</sub>	2.21 <sup>+0.25</sup> <sub>-0.46</sub>		
WISE J18+	-170 ± 30				<6250	0.5–2
WISE ToI 223	-100 ± 50				4750–5750	2–10
WISE ToI 268	-170 ± 30				<6000	5–50
WISE ToI 274	-30 ± 20				<6000	>10
WISE ToI 281	0 ± 50				<6250	>5
WISE ToI 1309	-30 ± 50	...	...			
WISE ToI 6	0 ± 50	...	...			
V391 Sct	-20 ± 40	...	...			

**Notes.** The three stars V391 Sct, WISE ToI 6, and WISE ToI 1309 do not show strong CO absorption features.

<sup>a</sup> Radial velocity of the RCB star, rounded to the nearest 50 km s<sup>-1</sup>.

<sup>b</sup> Quantities derived from modeling of maximum-light SEDs (Section 5.1.1).

<sup>c</sup> Quantities derived from NIR spectral modeling (Section 5.1.2).

irrespective of the dust contribution of the star. Figure 9 shows the best-fit synthetic spectra, together with the continuum-normalized NIR spectra. The five RCB stars WISE J17+, WISE J18+, WISE ToI 223, ASAS-RCB-21, and WISE ToI 268 show the strongest <sup>12</sup>C/<sup>18</sup>O absorption features. The first three are consistent with having <sup>16</sup>O/<sup>18</sup>O in the range 0.5–10, while ASAS-RCB-21 and WISE ToI 268 are consistent with <sup>16</sup>O/<sup>18</sup>O in 2–50 and 5–50, respectively (higher value for higher assumed dust contribution). Using the temperature range for NSV 11154 derived in Section 5.1.1, we constrain the <sup>16</sup>O/<sup>18</sup>O ratio in the range 10–50. For the remaining stars, the <sup>12</sup>C/<sup>18</sup>O absorption is weaker. Given the uncertainty in the dust contribution, we cannot put similar constraints on the <sup>16</sup>O/<sup>18</sup>O of these stars using our medium-resolution spectra. For these stars, we only indicate a lower limit on the oxygen isotope ratios from our fits. Table 3 lists the derived effective temperature constraints and oxygen isotope ratio ranges. In Section 5.1.1, we modeled the SEDs of four of the nine stars analyzed here (AO Her, NSV 11154, WISE J17+, and ASAS-RCB-21). We note that the temperatures derived from SED modeling are consistent with the constraints derived from NIR spectra.

The high <sup>18</sup>O abundances in RCB stars could be key to identifying their formation mechanism. The reaction <sup>14</sup>N( $\alpha$ ,  $\gamma$ ) F<sup>18</sup>( $\beta^+$ )<sup>18</sup>O is an important channel for synthesizing <sup>18</sup>O. The cores of intermediate-mass stars just before He burning commences can reach the temperatures required for this reaction (Warner 1967; Crawford et al. 2020). However, if a star undergoes a final helium flash, the temperature becomes high enough for all <sup>18</sup>O to be destroyed. The FF scenario is thus unlikely to explain the high <sup>18</sup>O abundances (García-Hernández et al. 2009). On the other hand, dynamically accreting material in mergers of CO- and He-core WDs can be sites for the synthesis of <sup>18</sup>O (Clayton et al. 2007). Jeffery et al. (2011) suggested that even a cold WD merger (i.e., without any nucleosynthesis) could explain the large quantities of <sup>18</sup>O in the remnant. These merger models successfully predict the high <sup>12</sup>C/<sup>13</sup>C ratio observed for most RCB stars (Asplund et al. 2000). Most RCB stars are thus thought to be formed from the

DD channel. García-Hernández et al. (2010) suggested that the DD scenario could link RCB stars with hydrogen-deficient carbon (HdC) stars. This is supported by the high <sup>18</sup>O abundances measured in HdC stars (Clayton et al. 2005).

There are a few challenges to the DD picture. Lithium has been detected in the spectra of one HdC (Rao & Lambert 1996) and four RCB stars (Asplund et al. 2000). The RCB stars VCrA, V854 Cen, VZ Sgr, and UX Ant have a high <sup>13</sup>C abundance (Rao & Lambert 2008; Hema et al. 2017). The presence of Li and <sup>13</sup>C in these stars was considered to be inconsistent with DD models and instead favorable for the FF scenario (Asplund et al. 2000; Clayton 2012). However, recently, Crawford et al. (2020) showed that it is possible to produce the required Li abundances in WD merger models for specific ranges of helium-burning temperatures. None of these anomalous RCB stars have an <sup>18</sup>O abundance measurement, as most of them are warm.

Oxygen isotope ratios have been previously measured for six known Galactic RCB stars and three HdC stars (Clayton et al. 2007; García-Hernández et al. 2009, 2010; Bhowmick et al. 2018). We have reported constraints on the ratios of six more RCB stars and provided lower limits for three RCB stars. Figure 10 shows a histogram of <sup>16</sup>O/<sup>18</sup>O ratios for all of these RCB stars. We also indicate ratios for the two HdC stars and mark the solar <sup>16</sup>O/<sup>18</sup>O value. The oxygen isotope ratios in the six RCB stars are at least an order of magnitude lower than the solar value. These stars also do not show any <sup>13</sup>C/<sup>16</sup>O features, further indicating that they originate in a WD merger. Additional NIR spectroscopic observations that populate this diagram will provide clues to the evolutionary channels of RCB stars. In particular, measuring the isotope ratios for anomalous cold RCB stars will help illuminate the multiple possible channels for RCB formation.

## 5.2. Pulsation Periods and Effective Temperatures

At maximum light, some RCB stars are known to pulsate with periods between 40 and 100 days and amplitudes of a few magnitudes (Lawson & Cottrell 1997). These pulsations can be

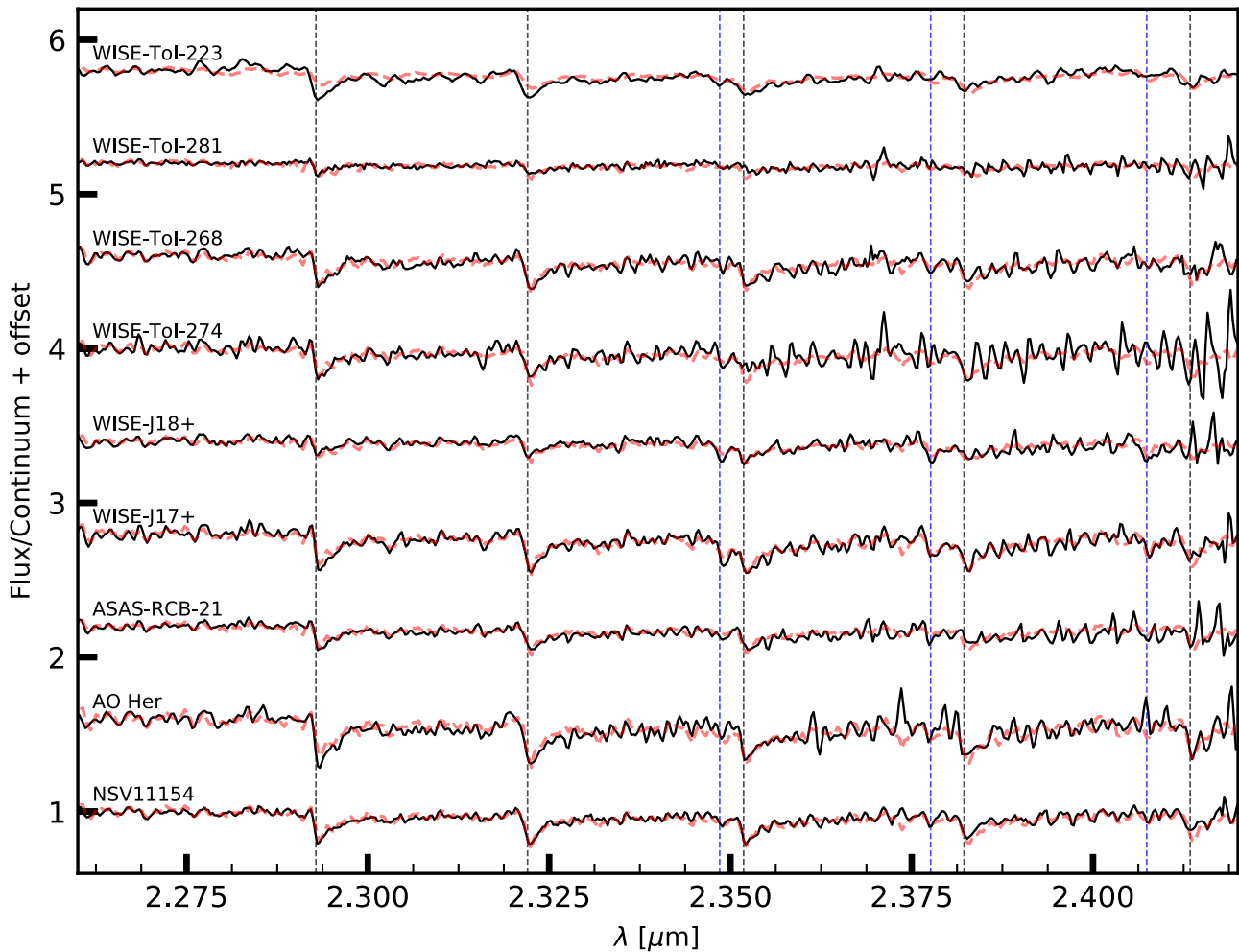


**Figure 9.** Best fits to the K-band spectra of RCB stars. The continuum-normalized spectra are plotted as black solid lines, and the best-fit synthetic spectra are plotted as red dashed lines. We mark the positions of the  $^{12}\text{C}^{16}\text{O}$  (black lines) and  $^{12}\text{C}^{18}\text{O}$  (blue lines) absorption band heads. The derived ranges of the best-fit temperatures and oxygen isotope ratios are listed in Table 3.

fairly irregular; the star can exhibit multiple pulsation modes or undergo changes in the dominant period. The star RCrB has shown pulsations with periods of 33, 44, 52, and 60 days (Lawson & Kilkenny 1996). Saio (2008) suggested that these semiregular or irregular pulsations can be explained by the onset of the strange instability in the remnant of a WD merger. They also found that longer-period ( $P > 100$  days) nonradial modes could be excited in these stars. Using WD merger models, they found that pulsation periods, together with the effective temperatures of RCB stars, can be indicative of their mass. These values have been measured previously for only three RCB stars: RCrB, RY SGr, and UW Cen.

The high-cadence PGIR light curves are ideal for identifying maximum-light pulsations in RCB stars. Of the 19 RCB stars analyzed in this paper, we can measure pulsations for five: AO Her, NSV 11154, V391 Sct, WISE J18+, and WISE ToI 8. Four of these are previously known RCB stars, but their pulsation periods and temperatures have not been reported. The star WISE J18+ has the most well-defined period of 41 days with an LS score of 0.4. The star AO Her shows a period of 56 days (LS score = 0.2) but with significant scatter that could be partly attributed to nonlinearity effects in the PGIR detector. For NSV 11154, we detect two distinct pulsation modes. The light curve shows one full cycle with a period of 96 days

(LS score = 0.5), followed by another cycle with a period of 48 days (LS score = 0.5) and a slightly smaller amplitude. It is possible that the first period is an overtone of the second. The star V391 Sct shows a full cycle with a period of 124 days (LS score = 0.4), and WISE ToI 8 shows a period of 30 days at low significance (LS score = 0.13).

Using our NIR spectra, we have put constraints on the effective temperatures of three of these stars: AO Her, NSV 11154, and WISE J18+ (Table 3). The star WISE ToI 8 shows several strong emission lines, suggesting that it has  $T_{\text{eff}} > 10,000$  K. Tisserand et al. (2013) suggested that V391 Sct has  $T_{\text{eff}} > 7500$  K based on the presence of metal absorption lines in its spectrum. In Figure 11, we plot the periods of these stars against their effective temperatures. This figure is similar to Figure 32 of Lawson et al. (1990) and Figure 15 of Rao & Lambert (2015).

### 5.3. Dust-driven Winds in RCB Stars

Clayton et al. (2003) showed that most (if not all) RCB stars have winds. These winds are thought to be driven by the dust surrounding the star. The RCB stars undergo frequent dust formation episodes (a photometric decline results if dust condenses along the line of sight to the star). Radiation pressure from the star can accelerate these dust particles to supersonic

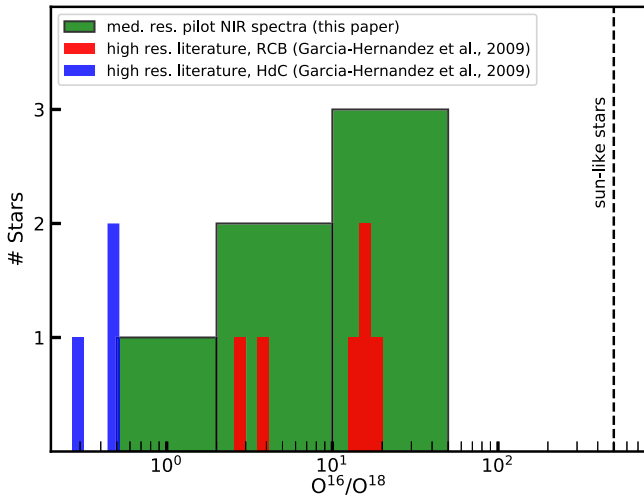


**Figure 10.** Distribution of  $^{16}\text{O}/^{18}\text{O}$  ratios of RCB and HdC stars. In red, we plot all six previously available measurements of the isotope ratios in RCB stars derived from high-resolution spectra (García-Hernández et al. 2009). In this paper, we report preliminary constraints on  $^{16}\text{O}/^{18}\text{O}$  for four new RCB stars. We indicate these new measurements in green. We note that five additional RCB stars reported in this paper show weak  $^{12}\text{C}^{18}\text{O}$  absorption features and are consistent with  $^{16}\text{O}/^{18}\text{O} > 10$ . In blue, we plot the isotope ratios measured for HdC stars, taken from García-Hernández et al. (2009). The high  $^{18}\text{O}$  content of RCB stars compared to Sun-like stars favors a WD merger origin for them. Further NIR spectroscopic observations that populate this diagram will provide additional clues about the formation channels of RCB stars.

velocities. The dust particles drag the gas along with them, giving rise to a wind. Consequently, HdC stars—close relatives of RCB stars that do not undergo major dust formation episodes—are not expected to show such winds.

The helium  $\lambda 10830$  line is an important tracer of winds in RCB stars for the following reasons: (1) helium is the most abundant element in RCB stars, and (2) the upper level for this line is 20 eV above the ground state and is thus unlikely to be populated by photospheric radiation of F- to G-type RCB stars. However, this level can be populated by collisional excitation in high-velocity winds around these stars. Clayton et al. (2003) first observed this line and noted its ubiquitous presence in RCB stars in their sample. While some stars show a clear P Cygni profile, most show only a strong blueshifted absorption component, as the emission component is affected by other photospheric absorption. They model these profiles to find wind velocities of  $200\text{--}350\text{ km s}^{-1}$  with column densities of  $10^{12}\text{ cm}^{-2}$ . Clayton et al. (2013) observed a larger sample and noted that the winds are usually strongest when the RCB is undergoing a decline.

Our NIR spectroscopic campaign is ideal to monitor the He I  $\lambda 10833$  line in a number of RCB stars in various evolutionary phases. Similar to Clayton et al. (2003) and Clayton et al. (2013), we detect strong He I features in the spectra of all RCB stars analyzed in this paper. Of the 19 total RCB stars analyzed, seven are in a deep decline and show the helium line only in emission. As these stars do not have any other spectral features, we cannot measure their radial velocities. We are thus unable to measure the wind velocities for these seven stars. Figure 12 shows the line profiles for the remaining 12 RCB stars. We note that some stars show terminal velocities as high as  $400\text{--}500\text{ km s}^{-1}$ . Such high He I velocities were reported previously by Clayton et al. (2013) for some RCB stars in

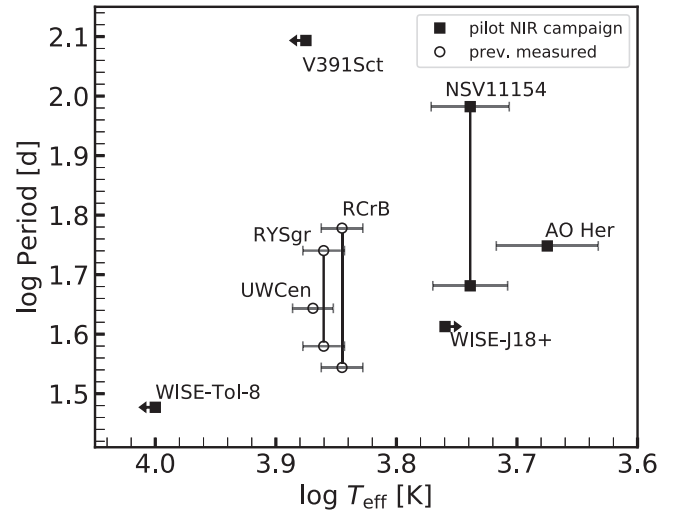


**Figure 11.** Pulsation periods against effective temperatures for RCB stars. The open circles indicate the three previously known positions of the RCB stars (RCrB, RY Sgr, and UW Cen) in this diagram. The filled circles indicate the RCB stars analyzed in this paper. The positions of the RCB stars in this diagram can be compared to WD merger models to infer the masses of the remnants (cf. Saio 2008).

their sample. We will present a detailed analysis of the He I profiles in a future paper.

#### 5.4. Radial Velocities of RCB Stars

The distribution of RCB stars and their velocities will shed further light on their formation channels. Of the 19 RCB stars (11 new + 8 previously known) analyzed in this paper, we measure radial velocities for eight by cross-correlating the barycentric velocity-corrected  $J$ - and  $K$ -band spectral orders separately with synthetic spectra (see Section 5.1.2). Three additional RCB stars were in the decline phase but showed weak C I absorption lines in the  $J$  band. We use these lines to measure the radial velocities for these stars. The measured radial velocities are listed in Table 3. Figure 13 shows a histogram of the measured velocities. In the figure, we also indicate the velocity measurements of other known RCB stars from the Gaia DR2. We note that the stars AO Her and NSV 11154 have particularly high radial velocities ( $\gtrsim 300\text{ km s}^{-1}$ ). Such high velocities could be indicative that these stars could be part of a halo population. Additional measurements that probe the velocity distribution of RCB stars will provide better insight about their formation mechanisms.

## 6. Summary and Way Forward

The population of RCB stars in the Milky Way is largely unexplored; only about a third of Galactic RCB stars are currently known. A systematic census of RCB stars is necessary to shed light on the nature of these mysterious objects. Major advances in this direction were made by Tisserand et al. (2020) with a catalog of 2194 WISE sources expected to contain  $\approx 85\%$  of the RCB stars in the Milky Way. In this paper, we used data from the PGIR, a  $J$ -band time domain survey, to prioritize this catalog for spectroscopic follow-up. Of the candidates, 1209 have PGIR coverage, of which 922 are above the sensitivity of the PGIR. Based on their light curves, we assigned a “light curve-based priority” to each of the 922 candidates. The top priority comprises 149

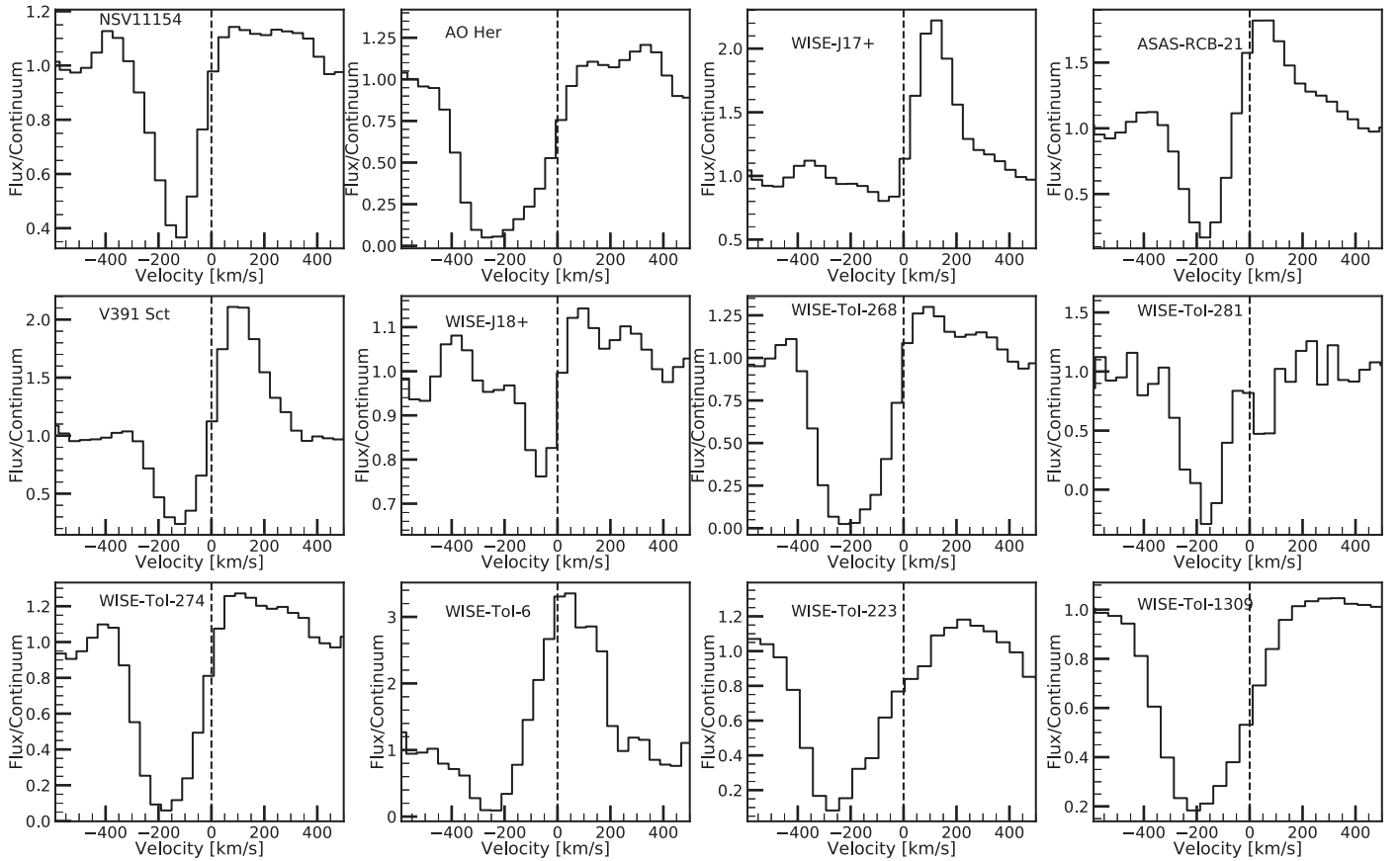


**Figure 12.** The He I  $\lambda 10830$  line profiles of the RCB stars analyzed in this paper. The helium line is an almost ubiquitous feature of RCB stars. This line originates in high-velocity winds in the atmospheres of these stars. Some RCB stars show a fully developed P Cygni profile, while some stars show only the blueshifted component. In the latter case, other photospheric absorption reduces the emission component. Here we have excluded the seven RCB stars that are in a dust-enshrouded dip, as we cannot derive radial velocities for them. These stars show the helium line in emission. The absorption component is absent, as almost all of the continuum is extinguished due to dust.

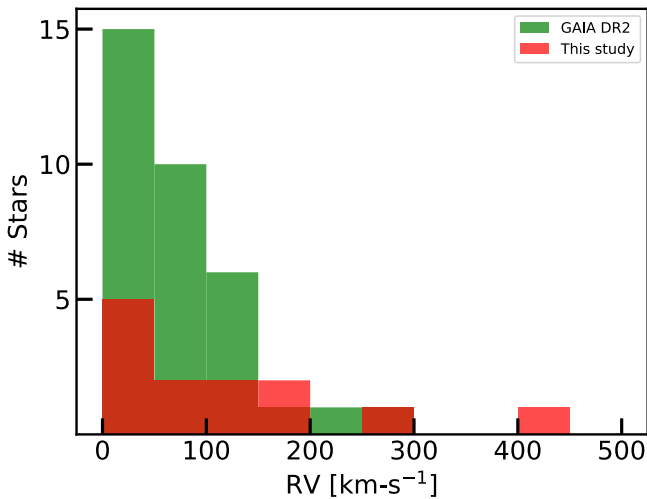


**Figure 13.** Distribution of the radial velocities of RCB stars. Previously known velocity measurements from Gaia DR2 are plotted in green, and measurements from this study are plotted in red. We note that two RCB stars have very high radial velocities ( $\gtrsim 300 \text{ km s}^{-1}$ ), which could be indicative of a halo population for these objects.

candidates that show light curves similar to RCB stars. The lowest priority consists of 272 candidates that we classified as LPVs and 23 as RV Tauri stars. Using our light curve-based classification, we identified IR color-based criteria that help

separate the RCB stars from the LPVs. We then assigned a second “color-based priority” to each of the 2194 candidates in the catalog. These priorities will aid the process of spectroscopic follow-up and maximize the yield of RCB stars.

We then obtained NIR spectra for eight known RCB stars and 26 of our top light curve-based priority RCB candidates. This was a pilot run for the first NIR spectroscopic campaign to identify RCB stars. We spectroscopically confirmed 11 new RCB stars and analyzed the NIR spectral features of these stars. In particular, we report constraints on the effective temperatures and oxygen isotope ratios for these stars. These quantities serve as useful diagnostics about the compositions and formation mechanisms of RCB stars. We derive maximum-light pulsation periods for five RCB stars and plot them in the period-effective temperature space. The position of an RCB star in this phase space can be used to derive the mass of the RCB star. Although the sample analyzed in this pilot run is small, it is indicative of the potential of a full NIR spectroscopic campaign for classifying RCB stars.

It is evident that NIR searches promise to be productive in identifying and characterizing RCB stars. The NIR time domain surveys are particularly well suited to discover highly dust-enshrouded RCB stars and those lying in highly extinguished regions of the Galactic bulge and plane. The light curve- and color-based priorities identified in this paper will help identify the remaining RCB stars in the Tisserand et al. (2020) catalog. We aim to complete the spectroscopic follow-up of the top candidates

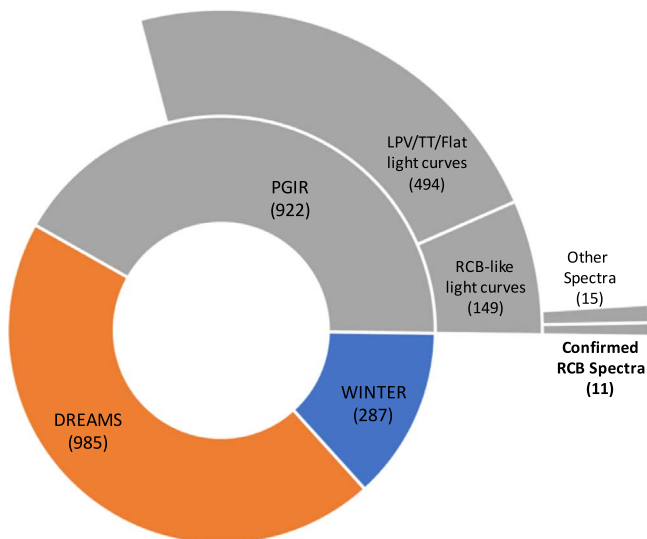


**Figure 14.** Schematic of our strategy for an NIR survey of Galactic RCB stars focusing on the Tisserand et al. (2020) catalog. Of the candidates from this catalog, 1209 are accessible from the Northern Hemisphere. Of these, 922 candidates are bright enough to be characterized by the PGIR. The remaining 287 fainter candidates will be characterized by WINTER, a deeper ( $J \approx 20$ ) NIR time domain survey starting in 2021 December. The candidates in the Southern Hemisphere will be characterized by DREAMS, an analog of WINTER in Australia.

in these priority classes. Further observations from the PGIR will help improve the light curve-based classifications for the (922) bright candidates visible in the Northern Hemisphere. The successor to the PGIR in the Northern Hemisphere is the Wide-field Infrared Transient Explorer (WINTER; Simcoe et al. 2019), a more sensitive  $J$ -band time domain survey (limiting  $J \approx 20$  mag). WINTER will start operating at Mt. Palomar by 2021 December and will help characterize the (287) fainter candidates in the Northern Hemisphere. The Dynamic Red All-sky Monitoring Survey (DREAMS) will be an analog of WINTER in the Southern Hemisphere at the Siding Springs Observatory. DREAMS will help characterize the 985 candidates that are accessible only from the south. Figure 14 shows a schematic of this strategy for our NIR census of RCB stars.

Moreover, systematic blind searches using data from these telescopes will help discover RCB stars outside this catalog. This includes the more exquisite RCB stars with double dust shells around them (Montiel et al. 2018) and DY Per stars, the colder cousins of RCB stars (Bhowmick et al. 2018). The NIR census thus promises to uncover the Galactic RCB population.

We thank our referee, Geoff Clayton, for valuable feedback that improved the manuscript. The Palomar Gattini IR (PGIR) is generously funded by Caltech, Australian National University, the Mt. Cuba Foundation, the Heising Simons Foundation, and the Binational Science Foundation. The PGIR is a collaborative project among Caltech, Australian National University, the University of New South Wales, Columbia University, and the Weizmann Institute of Science. M.M.K. acknowledges generous support from the David and Lucile Packard Foundation. J.S. acknowledges the support of an Australian Government Research Training Program (RTP) scholarship. Some of the data presented here were obtained with the Visiting Astronomer facility at the Infrared Telescope Facility, which is operated by the University of Hawaii under contract 80HQTR19D0030 with the National Aeronautics and Space Administration.

## ORCID iDs

Viraj R. Karambelkar <https://orcid.org/0000-0003-2758-159X>  
 Mansi M. Kasliwal <https://orcid.org/0000-0002-5619-4938>  
 Shreya Anand <https://orcid.org/0000-0003-3768-7515>  
 Michael C. B. Ashley <https://orcid.org/0000-0003-1412-2028>  
 Matthew Hankins <https://orcid.org/0000-0001-9315-8437>  
 Jacob E. Jencson <https://orcid.org/0000-0001-5754-4007>  
 Eran O. Ofek <https://orcid.org/0000-0002-6786-8774>  
 Roger M. Smith <https://orcid.org/0000-0001-7062-9726>  
 Roberto Soria <https://orcid.org/0000-0002-4622-796X>  
 Samaporn Tinyanont <https://orcid.org/0000-0002-1481-4676>  
 Yuhan Yao <https://orcid.org/0000-0001-6747-8509>

## References

- Alcock, C., Allsman, R. A., Alves, D. R., et al. 2001, *ApJ*, 554, 298  
 Alvarez, R., & Plez, B. 1998, *A&A*, 330, 1109  
 Amaro-Seoane, P., Audley, H., Babak, S., et al. 2017, arXiv:1702.00786  
 Asplund, M., Gustafsson, B., Lambert, D. L., & Rao, N. K. 2000, *A&A*, 353, 287  
 Bailer-Jones, C. A. L., Rybizki, J., Founesneau, M., Mantelet, G., & Andrae, R. 2018, *AJ*, 156, 58  
 Bell, R. A., Eriksson, K., Gustafsson, B., & Nordlund, A. 1976, *A&As*, 23, 37  
 Bhowmick, A., Pandey, G., Joshi, V., & Ashok, N. M. 2018, *ApJ*, 854, 140  
 Burdge, K. B., Prince, T. A., Fuller, J., et al. 2020, *ApJ*, 905, 32  
 Clayton, G. C. 1996, *PASP*, 108, 225  
 Clayton, G. C. 2012, *JAVSO*, 40, 539  
 Clayton, G. C., Geballe, T. R., & Bianchi, L. 2003, *ApJ*, 595, 412  
 Clayton, G. C., Geballe, T. R., Herwig, F., Fryer, C., & Asplund, M. 2007, *ApJ*, 662, 1220  
 Clayton, G. C., Geballe, T. R., & Zhang, W. 2013, *AJ*, 146, 23  
 Clayton, G. C., Herwig, F., Geballe, T. R., et al. 2005, *ApJL*, 623, L141  
 Clayton, G. C., Sugerman, B. E. K., Stanford, S. A., et al. 2011, *ApJ*, 743, 44  
 Clayton, G. C., Whitney, B. A., Stanford, S. A., & Drilling, J. S. 1992, *ApJ*, 397, 652  
 Crawford, C. L., Clayton, G. C., Munson, B., Chatzopoulos, E., & Frank, J. 2020, *MNRAS*, 498, 2912  
 Cushing, M. C., Vacca, W. D., & Rayner, J. T. 2004, *PASP*, 116, 362  
 De, K., Ashley, M. C. B., & Andreoni, I. 2020a, *ApJS*, 901, 1  
 De, K., Hankins, M. J., Kasliwal, M. M., et al. 2020b, *PASP*, 132, 025001  
 De Marco, O., Clayton, G. C., Herwig, F., et al. 2002, *AJ*, 123, 3387  
 Elitzur, M., & Ivezić, Ž. 2001, *MNRAS*, 327, 403  
 Feast, M. W., Carter, B. S., Roberts, G., Marang, F., & Catchpole, R. M. 1997, *MNRAS*, 285, 317  
 Foreman-Mackey, D., Hogg, D. W., Lang, D., & Goodman, J. 2013, *PASP*, 125, 306  
 Fryer, C. L., & Diehl, S. 2008, in ASP Conf. Ser. 391, Hydrogen-Deficient Stars, ed. A. Werner & T. Rauch (San Francisco, CA: ASP), 335  
 García-Hernández, D. A., Hinkle, K. H., Lambert, D. L., & Eriksson, K. 2009, *ApJ*, 696, 1733  
 García-Hernández, D. A., Lambert, D. L., Kameswara Rao, N., Hinkle, K. H., & Eriksson, K. 2010, *ApJ*, 714, 144  
 Geiss, J., Gloeckler, G., & Charbonnel, C. 2002, *ApJ*, 578, 862  
 Gezer, I., Van Winckel, H., Bozkurt, Z., et al. 2015, *MNRAS*, 453, 133  
 Grankin, K. N., Melnikov, S. Y., Bouvier, J., Herbst, W., & Shevchenko, V. S. 2007, *A&A*, 461, 183  
 Gustafsson, B., Bell, R. A., Eriksson, K., & Nordlund, A. 1975, *A&A*, 500, 67  
 Gustafsson, B., Edvardsson, B., Eriksson, K., et al. 2008, *A&A*, 486, 951  
 Han, Z. 1998, *MNRAS*, 296, 1019  
 Hema, B. P., Pandey, G., Kamath, D., et al. 2017, *PASP*, 129, 104202  
 Herter, T. L., Henderson, C. P., Wilson, J. C., et al. 2008, *Proc. SPIE*, 7014, 70140X  
 Iben, I., Tutukov, A. V., & Yungelson, L. R. 1996, in ASP Conf. Ser. 96, Hydrogen Deficient Stars, ed. C. S. Jeffery & U. Heber (San Francisco, CA: ASP), 409  
 Ivezić, Z., & Elitzur, M. 1997, *MNRAS*, 287, 799  
 Ivezić, Z., Nenkova, M., & Elitzur, M. 1999, arXiv:astro-ph/9910475  
 Jayasinghe, T., Kochanek, C. S., Stanek, K. Z., et al. 2018, *MNRAS*, 477, 3145  
 Jeffery, C. S., Karakas, A. I., & Saio, H. 2011, *MNRAS*, 414, 3599

- Karakas, A. I., Ruiters, A. J., & Hampel, M. 2015, *ApJ*, 809, 184
- Kijbunchoo, N., Clayton, G. C., Vieux, T. C., et al. 2011, *PASP*, 123, 1149
- Kilkenny, D., & Marang, F. 1989, *MNRAS*, 238, 1P
- Lawson, W. A., & Cottrell, P. L. 1989, *MNRAS*, 240, 689
- Lawson, W. A., & Cottrell, P. L. 1997, *MNRAS*, 285, 266
- Lawson, W. A., Cottrell, P. L., Kilmartin, P. M., & Gilmore, A. C. 1990, *MNRAS*, 247, 91
- Lawson, W. A., & Kilkenny, D. 1996, in ASP Conf. Ser. 96, Hydrogen Deficient Stars, ed. C. S. Jeffery & U. Heber (San Francisco, CA: ASP), 349
- Lee, C. H. 2015, *A&A*, 575, A2
- Lee, C.-H., Matheson, T., Soraisam, M., et al. 2020, *AJ*, 159, 61
- Lomb, N. R. 1976, *Ap&SS*, 39, 447
- Mathis, J. S., Rumpl, W., & Nordsieck, K. H. 1977, *ApJ*, 217, 425
- Montiel, E. J., Clayton, G. C., Sugerman, B. E. K., et al. 2018, *AJ*, 156, 148
- Moore, A. M., & Kasliwal, M. M. 2019, *NatAs*, 3, 109
- Morgan, D. H., Hatzidimitriou, D., Cannon, R. D., & Croke, B. F. W. 2003, *MNRAS*, 344, 325
- Otero, S., Hümmerich, S., Bernhard, K., & Sozynski, I. 2014, *JAVSO*, 42, 13
- Plez, B. 2008, *PhS*, 133, 014003
- Rao, N. K., & Lambert, D. L. 1996, in ASP Conf. Ser. 96, Hydrogen Deficient Stars, ed. C. S. Jeffery & U. Heber (San Francisco, CA: ASP), 43
- Rao, N. K., & Lambert, D. L. 2008, *MNRAS*, 384, 477
- Rao, N. K., & Lambert, D. L. 2015, *MNRAS*, 447, 3664
- Rayner, J. T., Toomey, D. W., Onaka, P. M., et al. 2003, *PASP*, 115, 362
- Ruiters, A. J., Belczynski, K., & Fryer, C. 2009, *ApJ*, 699, 2026
- Saio, H. 2008, in ASP Conf. Ser. 391, Hydrogen-Deficient Stars, ed. A. Werner & T. Rauch (San Francisco, CA: ASP), 69
- Scargle, J. D. 1982, *ApJ*, 263, 835
- Schlafly, E. F., & Finkbeiner, D. P. 2011, *ApJ*, 737, 103
- Shields, J. V., Jayasinghe, T., Stanek, K. Z., et al. 2019, *MNRAS*, 483, 4470
- Simcoe, R. A., Fűrész, G., Sullivan, P. W., et al. 2019, *AJ*, 157, 46
- Tisserand, P. 2012, *A&A*, 539, A51
- Tisserand, P., Clayton, G. C., Bessell, M. S., et al. 2020, *A&A*, 635, A14
- Tisserand, P., Clayton, G. C., Welch, D. L., et al. 2013, *A&A*, 551, A77
- Tisserand, P., Marquette, J. B., Beaulieu, J. P., et al. 2004, *A&A*, 424, 245
- Tisserand, P., Marquette, J. B., Wood, P. R., et al. 2008, *A&A*, 481, 673
- Tisserand, P., Wood, P. R., Marquette, J. B., et al. 2009, *A&A*, 501, 985
- Vacca, W. D., Cushing, M. C., & Rayner, J. T. 2003, *PASP*, 115, 389
- VanderPlas, J. T., & Ivezić, Ž. 2015, *ApJ*, 812, 18
- Warner, B. 1967, *MNRAS*, 137, 119
- Webbink, R. F. 1984, *ApJ*, 277, 355
- Zaniewski, A., Clayton, G. C., Welch, D. L., et al. 2005, *AJ*, 130, 2293